# Title: Susceptibility to Zika virus in a Collaborative Cross mouse strain is induced by *Irf3* deficiency *in vitro* but requires other variants *in vivo*, not linked to the type I interferon response

Short title: *Irf3* deficiency induces susceptibility to ZIKV *in vitro*, not *in vivo*

Marie Bourdon[§1], Caroline Manet[§1], Laurine Conquet[1], Corentin Ramaugé-Parra[1], Etienne Kornobis[2], Eliette Bonnefoy[3], Xavier Montagutelli[#1]

[1]Institut Pasteur, Université de Paris, Mouse Genetics Laboratory, F-75015 Paris, France

[2]Institut Pasteur, Université de Paris, Biomics, F-75015 Paris, France

[3]Université Paris Cité, Institut Cochin, Inserm, CNRS, F-75014 Paris, France

[§] M.B. and C. M. equally contributed to this work and are co-first authors

[#] Corresponding author: xavier.montagutelli@pasteur.fr

Keywords: Zika virus, mouse, Irf3, interferon response, Collaborative Cross

**Abstract**

Zika virus (ZIKV) is a Flavivirus responsible for recent epidemics in Pacific Islands and in the Americas. In humans, the consequences of ZIKV infection range from asymptomatic infection to severe neurological disease such as Guillain-Barré syndrome or fetal neurodevelopmental defects, suggesting, among other factors, the influence of host genetic variants. We previously reported similar diverse outcomes of ZIKV infection in mice of the Collaborative Cross (CC), a collection of inbred strains with large genetic diversity. CC071/TauUnc (CC071) was the most susceptible CC strain with severe symptoms and lethality. Notably, CC071 has been recently reported to be also susceptible to other flaviviruses including dengue virus, Powassan virus, West Nile virus, and to Rift Valley fever virus. To identify the genetic origin of this broad susceptibility, we investigated ZIKV replication in mouse embryonic fibroblasts (MEFs) from CC071 and two resistant strains. CC071 showed uncontrolled ZIKV replication associated with delayed induction of type-I interferons (IFN-I). Genetic analysis identified a mutation in the *Irf3* gene specific to the CC071 strain which prevents the protein phosphorylation required to activate interferon beta transcription. We demonstrated that this mutation induces the same defective IFN-I response and uncontrolled viral replication in MEFs as an *Irf3* knock-out allele. By contrast, we also showed that *Irf3* deficiency did not induce the high plasma viral load and clinical severity observed in CC071 mice and that susceptibility alleles at other genes, not associated with the IFN-I response, are required. Our results provide new insight into the *in vitro* and *in vivo* roles of *Irf3*, and into the genetic complexity of host responses to flaviviruses.

**Author summary**

Recent ZIKV outbreaks led to millions of infected people, with rare but severe complications such as Guillain-Barré syndrome and encephalitis in adults suggesting that host genes

influence the susceptibility to severe forms of infection. We previously reported the importance of host genes in ZIKV pathogenesis using a panel of genetically diverse mouse strains and identified CC071 as the most susceptible strain. Importantly, this mouse strain has been shown by others to be also susceptible to several other RNA viruses. Through a combination of functional and genetic approaches in a cellular model, we identified a mutation in the *Irf3* gene which plays a key role in activating the expression of interferon beta to induce the type I interferon response, the first line of host defense against the virus. This mutation fully explains the high viral replication observed in CC071 cells. However, it was not able to induce the elevated viremia and the symptoms displayed by CC071 ZIKV-infected mice, unraveling the implication of other host genes which are not associated with the type I interferon response. Because of the broad susceptibility of CC071 to multiple viruses, our results have implications beyond ZIKV infection and contribute to shedding light on the plurality of host mechanisms fighting infectious diseases.

57 **Introduction**

58 Zika virus (ZIKV) is a mosquito-borne virus of the *Flaviviridae* family identified in 1947 in
59 Uganda. The first noticeable human outbreaks occurred in Micronesia in 2007 and in French
60 Polynesia and New Caledonia in 2013-2014. In 2015-2016, ZIKV caused an epidemic in Brazil
61 which rapidly spread across the Americas and the Caribbean. To date, 89 countries have
62 reported evidence of mosquito-transmitted Zika virus infection (https://www.who.int/health-
63 topics/zika-virus-disease#tab=tab_1).

64 While most people infected with ZIKV remain asymptomatic, some develop non-specific
65 symptoms including rash, fever, conjunctivitis, muscle and joint pain, malaise and headache.
66 Neurological complications have been described in adults such as Guillain-Barré syndrome (1)
67 and encephalitis (2). Infection of pregnant women was associated with congenital Zika
68 syndrome in the fetus, which can lead to neurodevelopmental deficiencies, brain
69 malformation (3) or in some cases to fetal loss (4).

70 Many factors may contribute to this variable severity, including the viral strain, the infection
71 route and dose, and the host genetic background (5,6). Indeed, mouse and human studies
72 have shown that host genes influence flaviviral infections' outcomes (7). While human genetic
73 studies are hampered by the variability of these multiple factors, they can be controlled in
74 mouse models which have proven very valuable to identify susceptibility variants (8,9).
75 Relevant ZIKV infection models have been developed in mice either using *Ifnar1* knock-out
76 (KO) mice in which the IFNAR receptor to IFN-I has been inactivated (10,11), or by blocking
77 this receptor using a monoclonal antibody targeting the IFNAR1 receptor subunit (MAR1-5A3
78 (12)).

79 We have previously explored the role of mouse natural genetic variants on ZIKV susceptibility
80 in the Collaborative Cross (CC), a panel of recombinant inbred mice encompassing a genetic

diversity similar to that of the human population and capturing approximately 90% of the mouse natural genetic variants (13,14). We reported that the CC genetic diversity enabled large variations in the clinical severity of ZIKV disease, plasma viral load and intensity of brain pathology, comparable to those observed in human cases (15). We specifically identified CC071/TauUnc (CC071) mice as very susceptible, with high mortality and high peak plasma viral load. Notably, the CC071 strain has been recently reported as also susceptible to other flaviviruses including dengue virus (15), Powassan virus (16), West Nile virus (WNV) (15), and to Rift Valley fever virus (17), emphasizing its value to decipher genetic factors controlling host responses to RNA viruses.

We previously demonstrated that genetic background influenced ZIKV replication in CC mouse embryonic fibroblasts (MEFs). Here, we investigated the mechanisms driving high viral replication in CC071 MEFs. We found that, compared with the more resistant C57BL/6J (B6) and CC001/Unc (CC001) strains, ZIKV-infected CC071 MEFs displayed a delayed expression of the IFN-I response genes. Genetic and functional analyses identified a strain-specific variant in the *Irf3* gene, the first transcription factor involved in interferon (IFN) β expression, which mimics the effects of a null allele *in vitro* and fully explains the delayed IFN-I expression and uncontrolled viral replication. By contrast, we showed, from the *in vivo* comparison of CC071, *Irf3*-deficient and backcross mice, that the CC071 *Irf3* mutation is not sufficient to explain the high susceptibility of CC071 mice to ZIKV infection and that other genes, not associated with the IFN-I response, are involved. These findings provide new insights into the roles of *Irf3* in viral diseases and exemplify how the study of CC strains allows deciphering the role of host genes in viral pathogenesis.

104 **Results**

105 *CC071 MEFs show defective control of viral replication and delayed IFN-I expression, but*
106 *normal response to IFN-I stimulation*

107 We previously reported that, unlike CC001 MEFs, CC071 MEFs produced increasing quantities
108 of viral particles during the first 72 hours post-infection (hpi) (15). Here, we confirmed and
109 expanded this observation by infecting B6, CC001 and CC071 MEFs and by quantifying viral
110 particles by FFA. After ZIKV infection, CC071 MEFs displayed high and increasing viral titers
111 between 24 and 72 hpi, while CC001 and B6 MEFs showed stable and lower titers (Fig 1A).

112 To investigate the origin of the defective control of viral replication in CC071 MEFs, we
113 measured the expression level of the *Ifnb1* gene coding for IFNβ in ZIKV-infected CC071, CC001
114 and B6 MEFs. *Ifnb1* expression is induced very rapidly after virus detection by sensors and
115 triggers the innate antiviral response which is essential for limiting viral replication. In CC001
116 and B6 MEFs, *Ifnb1* expression was significantly induced at 24 hpi and remained stable and
117 high until at least 72 hpi (Fig 1B). In contrast, its expression in CC071 MEFs was low at 24 hpi
118 and reached the level of CC001 only at 72 hpi. Similar results were obtained for *Ifn4a* which
119 encodes one of the IFNα proteins (Sup Fig 1). Notably, *Ifnb1* expression in CC071 MEFs at 72
120 hpi was significantly higher than in B6 MEFs, showing that CC071 MEFs were delayed but not
121 intrinsically hampered in their ability to induce strong IFN-I expression.

122 To test whether this defective induction of *Ifnb1* expression was specific to ZIKV infection,
123 MEFs were then transfected with the influenza A virus-derived 3-phosphate-hairpin-RNA (3p-
124 hpRNA), an agonist of the RIG-I/MDA5-MAVS pathway, or treated with polyinosine-
125 polycytidylic acid (poly (I:C)), that activates both Toll-like receptor (TLR) 3 (TLR3) and the RIG-
126 I/MDA5-MAVS pathway (18). Here again, CC071 MEFs showed a delayed expression of *Ifnb1*
127 after both stimulations by comparison with B6 and CC001 MEFs (Sup Fig 2), indicating that the

128 defect in IFN-I genes expression in CC071 MEFs was not specific to ZIKV infection. This result
129 suggested a defect in the molecular cascade between cellular sensors of pathogen-associated
130 molecular patterns (PAMP) and the *Ifnb1* gene transcription machinery.
131 To evaluate the capacity of CC071 MEFs to respond to IFN-I, they were treated with
132 recombinant IFN$\alpha$. The expression of IFN-stimulated genes (ISGs) such as *Ifitm3* was induced
133 with the same kinetics and level as in B6 and CC001 MEFs (Fig 1C), showing that CC071 MEFs
134 are able to respond normally to IFN-I stimulation and that their defect is limited to the
135 induction of *Ifnb1* gene expression.
136
137 *CC071's delayed Ifnb1 expression is strain-specific*
138 To gain insight into the mechanisms responsible for defective *Ifnb1* induction, we investigated
139 the expression levels of all genes involved in *Ifnb1* expression on CC071, B6 and CC001 MEFs
140 at 16, 24 and 32 hpi. Mock-infected MEFs were analyzed at 24 hours as controls. Expression
141 levels were measured by RNA sequencing (RNAseq) which provided a comprehensive analysis
142 of transcriptomic changes. In CC001 MEFs, the expression of many genes rapidly increased
143 after infection (160 at 16h, 821 at 24h and 971 at 32h; log2 fold-change > 1, FDR = 0.05),
144 reflecting a robust innate antiviral response (Sup Fig 3A). A similar pattern was observed in B6
145 MEFs. By contrast, the expression of only 38 genes was increased in CC071 MEFs at 32hpi (34
146 of which were also activated in CC001), consistent with the delayed induction of *Ifnb1*
147 expression. Among the genes that are involved in the pathway between PAMP sensors and
148 *Ifnb1* transcription, ISGs such as *Tlr3*, *Ddx58* (coding for RIG-I sensor) or *Irf7* were not activated
149 upon infection in CC071, while constitutively expressed genes such as *Mavs*, *Ticam1* (coding
150 for the TRIF adaptor), *Traf3* or *Irf3*, showed comparable levels of expression in the three

151 strains (Sup Fig 3B). Therefore, this analysis did not provide new clues for identifying the gene
152 responsible for the defect observed in CC071.
153 We then leveraged the genetic architecture of the CC which genomes are patchworks of
154 haplotypes inherited from the eight founder strains (19). Although CC071 was the only strain
155 with severe ZIKV disease, we hypothesized that, if the delayed activation of *Ifnb1* resulting in
156 uncontrolled viral replication observed in CC071 MEFs was due to an allele at one of the genes
157 involved in the *Ifnb1* induction pathway inherited from a parental strain, ZIKV-infected MEFs
158 of CC strains carrying the same allele would present similarly high viral titers. We therefore
159 derived MEFs from each CC strain available to us carrying the same ancestral haplotype as
160 CC071 at one of the 13 genes of the pathway (Fig 2A). Upon ZIKV infection, none of these CC
161 MEFs showed viral titer kinetics resembling that observed in CC071 MEFs (Fig 2B). These
162 results suggested two alternative hypotheses. Either the delayed *Ifnb1* activation involved two
163 members of the pathway with a CC071-specific allelic combination leading to a non-functional
164 interaction, or CC071 was carrying a strain-specific allele at one of these genes, resulting from
165 a mutation proper to CC071 that probably arose on an ancestral haplotype during the CC071
166 inbreeding. However, the sequencing of one male of each CC strain reported in 2017 (20) did
167 not identify such "private" variants with high predicted impact in CC071 for any of these genes.
168 Whatever the molecular mechanism, our results indicated that it was specific to CC071.
169
170 *Genetic analysis identifies Irf3 as a candidate gene in a haplotype shared between CC071 and*
171 *CC001*
172 We then turned to a genetic mapping approach. We first established that (CC001xCC071)F1
173 MEFs responded to infection with as rapid induction of *Ifnb1* expression as CC001 MEFs (Sup
174 Fig 4), suggesting that this CC071 trait was recessively inherited. F1 mice were therefore

175 backcrossed with CC071. MEFs were produced from each of 51 backcross (BC) embryos,
176 infected with ZIKV, and analyzed for viral titer and *Ifnb1* expression as above. One CC001 and
177 one CC071 MEF lines were included in each infection experiment as controls. BC MEFs
178 displayed either rapid and high *Ifnb1* expression with low viral titer (like CC001), or high viral
179 titer and delayed *Ifnb1* expression (like CC071, Fig 3A-B), showing that these two traits
180 correlated across the BC diverse genetic backgrounds.
181 To confirm this apparently binary distribution, we conducted linear discriminant analysis (LDA)
182 on CC001 and CC071 MEFs using *Ifnb1* expression at the three time points as variables.
183 Applying the LDA coefficients to backcross MEFs data classified individuals either in a CC001-
184 like group (n=31; 61%) or in a CC071-like group (n=20; 39%), with a mean probability of
185 prediction of 0.975 and 0.991, respectively (Fig 3C). Quantitative trait locus (QTL) mapping
186 was performed using LDA classification as a binary trait. Genome scan identified a peak on
187 chromosome 7 with a LOD (logarithm of the odd) score of 9.138 ($p < 0.001$, Fig 4A) located in
188 a region centered on the *Irf3* gene which, given its main role in the regulation of *Ifnb1*
189 expression, appeared as an obvious candidate. However, both CC001 and CC071 inherited the
190 CAST/EiJ haplotype in this region (Fig 4B), strongly suggesting that CC071's susceptibility was
191 caused by a variant proper to this strain.
192
193 *Abnormal splicing of Irf3 mRNA in CC071 leads to a loss of IRF3 transcriptional function*
194 To identify the CC071-specific mutation, we re-analyzed the RNAseq data and investigated the
195 splicing events between *Irf3* exons. As shown in Fig 5A, no splicing was observed between
196 exons 6 and 7 in CC071 MEFs, while a short cryptic exon was added to exon 6 (red box). This
197 aberrant splicing resulted in an mRNA lacking the last two exons. Notably, exon 8 encodes the
198 serin-rich region of the protein with the phosphorylation sites necessary for IRF3 activation

199 and nuclear translocation leading to *Ifnb1* transcription (Fig 5B). Neither long-range PCRs nor
200 sequencing could identify the exact nature of *Irf3* genetic alteration in CC071 but suggested
201 the insertion of a repeated sequence between exons 6 and 7. Nevertheless, the functional
202 consequence of this mutation was confirmed by Western blot using a specific C-terminal IRF3
203 antibody which showed that full-length IRF3 protein was absent in CC071 MEFs (Fig 5C).
204 Moreover, immunofluorescence using an antibody directed against phosphorylated IRF3
205 detected a positive signal in the nucleus of many ZIKV-infected CC001 and B6 MEFs, but not
206 in CC071 MEFs (Fig 5D). Altogether, these results show that CC071 carries a mutation in *Irf3*
207 that prevents IRF3 phosphorylation which is required to induce *Ifnb1* expression. Whether the
208 altered mRNA sequence prevents the production of the protein or alters its activity, this
209 mutation results in the loss of IRF3 transcriptional function.
210
211 CC071 *Irf3 mutation is responsible for uncontrolled viral replication in MEFs*
212 To test if the delayed *Ifnb1* expression resulting in uncontrolled viral replication in CC071 MEFs
213 was caused exclusively by the *Irf3* mutation, we performed a quantitative complementation
214 test by producing compound heterozygous MEFs carrying a knockout *Irf3* allele ($Irf3^{KO}$) and a
215 CC071 allele ($Irf3^{71}$). These $Irf3^{KO/71}$ MEFs were compared with CC071 and B6-$Irf3^{KO/KO}$ MEFs,
216 and with heterozygous MEFs carrying a B6 wildtype allele and either an $Irf3^{KO}$ or an $Irf3^{71}$ allele
217 ($Irf3^{+/KO}$ or $Irf3^{+/71}$, respectively, Fig 6A). While $Irf3^{+/KO}$ and $Irf3^{+/71}$ ZIKV-infected MEFs showed
218 the same pattern as CC001 or B6 MEFs (rapid induction of *Ifnb1* expression and controlled
219 viral replication, see Fig 1A for comparison), CC071 ($Irf3^{71/71}$), B6-$Irf3^{KO/KO}$ and $Irf3^{KO/71}$ MEFs
220 carrying two defective alleles at *Irf3* showed similar results (Fig 6B-C). These data demonstrate
221 that, since the $Irf3^{KO}$ did not complement the $Irf3^{71}$ allele, the *Irf3* mutation in CC071
222 contributes to the defects observed in ZIKV-infected MEFs. Moreover, since the data obtained

223 on CC071 and on *Irf3*$^{KO/71}$ MEFs were identical, we conclude that the CC071 *Irf3* mutation is
224 sufficient to induce the defects observed in CC071 MEFs.
225
226 *CC071 Irf3 mutation is not sufficient to explain susceptibility in vivo*
227 We investigated whether this *Irf3* mutation was also responsible for the high susceptibility to
228 ZIKV of CC071 mice. We first evaluated its effects in a context allowing IFN-I response. To this
229 aim, we compared B6, B6-*Irf3* KO and CC071 mice infected without prior MAR1-5A3
230 treatment, which results in moderate and short-lasting plasma viral loads without clinical
231 signs, as we previously reported (15). Similar viral loads were observed in B6 and B6-*Irf3* KO
232 mice at all days p.i. (dpi), while CC071 mice showed significantly higher viral loads at days 1
233 and 2 p.i. (Fig 7A). This result indicates that, unlike in MEFs, the *Irf3* null mutation does not
234 induce elevated viral replication *in vivo* (as measured by plasma viral load) and suggests that
235 CC071 mice carry susceptibility alleles at other loci.
236 We then blocked IFN-I response by pre-treating mice with MAR1-5A3 and compared peak
237 plasma viral load and clinical signs in ZIKV-infected B6, B6-*Irf3* KO and CC071 mice. While no
238 differences were observed between B6 and B6-*Irf3* KO mice (moderate plasma viral loads
239 without clinical signs), as expected if the IFN-I response is neutralized, CC071 mice developed
240 significantly higher viral loads at day 2 p.i. and signs of disease (ruffled fur, hunched posture
241 and body weight loss) around 7 days p.i. (Fig 7B). This contrast could result either from
242 functional differences between the *Irf3*$^{KO}$ and *Irf3*$^{71}$ alleles or from CC071 alleles at other genes
243 not linked with the IFN-I response. F1 mice between CC071 and B6-*Irf3* KO mice gave similar
244 results as B6-*Irf3* KO mice, suggesting that CC071 susceptibility alleles were recessive.
245 Therefore, we generated a small cohort of (CC071 x B6-*Irf3* KO) x CC071 backcross mice and
246 genotyped them for the *Irf3* gene by PCR using primers that amplify intron 6 of the *Irf3*$^{KO}$ allele,

247 but not of the *Irf3*$^{71}$ allele. (Fig 5A and Fig S5). We found no differences in plasma viral load
248 and clinical scores between *Irf3*$^{KO/71}$ and *Irf3*$^{71/71}$ backcross mice, indicating that the two alleles
249 are functionally equivalent *in vivo*. Moreover, *Irf3*$^{KO/71}$ backcross mice were more severely
250 affected than *Irf3*$^{KO/71}$ F1 mice, indicating the strong effects of recessive alleles from CC071
251 which likely explain the variability of plasma viral load and clinical signs among backcross mice.
252 Altogether, our results demonstrate that the CC071 mutation is a loss-of-function (LOF)
253 variant which does not confer susceptibility to ZIKV disease in the absence of other recessive
254 alleles carried by CC071 at genes not associated with the IFN-I response.
255

256 **Discussion**

257 An increasing number of publications have reported how the genetic diversity provided by the
258 CC translates into an extended range of resistant and susceptible phenotypes in various
259 infectious models. Since our first description of the high susceptibility of CC071 mice to ZIKV
260 infection, with disease severity and peak plasma viral load almost as high as those of B6-*Ifnar1*
261 KO mice, and higher clinical signs and mortality than 129-*Ifnar1* KO mice (15), several groups
262 have reported similar observations for other viruses. High viral load was found in CC071 mice
263 after dengue infection (15). Lethality after infection with West Nile virus (15) or Powassan
264 virus (16) were also described, although there is likely contribution from the defective *Oas1b*
265 allele that CC071 has inherited from 129S1/SvImJ. CC071 was also one of the most susceptible
266 CC strains to Rift Valley Fever virus infection (17) and to hepacivirus with long-term viral
267 persistence (21). Because of its unique genetic background, this strain will be increasingly
268 useful for infectious diseases studies, which underlines the importance of deciphering the
269 mechanisms of its susceptibility to each pathogen.

270 In this study, we leveraged from our previous observation that CC071 MEFs failed to control
271 ZIKV replication by comparison with resistant strains. Although they cannot recapitulate the
272 complex interactions between multiple pathways, cell types and tissues of a whole organism,
273 MEFs are a convenient cellular model which can be easily derived from any mouse genetic
274 background. We identified a delayed activation of the *Ifnb1* gene in CC071 MEFs, resulting in
275 delayed stimulation of ISGs. We then used a combination of genetic approaches to find the
276 causative gene defect. The observation that MEFs were normally responsive to IFN-I
277 stimulation was consistent with the higher susceptibility of mice treated by the MAR1-5A3
278 antibody compared with untreated mice which did not develop symptoms and showed much
279 lower plasma viral load (15). These results pointed at the pathway from PAMP sensors to *Ifnb1*

280 transcription factors. Transcriptional analysis did not identify reduced expression of non-ISGs
281 of this pathway. CC strains' genomic structure allows searching for haplotypes inherited from
282 the same founder in CC strains showing similar phenotypes. However, we did not identify such
283 haplotypes for genes of the *Ifnb1* induction pathway, suggesting that the defects observed in
284 CC071 MEFs were strain specific. It is finally the analysis of MEFs derived from backcross
285 embryos that established a monogenic inheritance, and genetic linkage unambiguously
286 pointed at the causative *Irf3* gene. The MEF experimental model was particularly appropriate
287 since we could derive cell lines from every backcross embryo. Our RNAseq data showed an
288 RNA splicing defect in the *Irf3* gene in CC071, which functional consequences could be
289 validated *in vitro*. The formal proof that the CC071 *Irf3* mutation was necessary and sufficient
290 to cause *Ifnb1* delayed activation and uncontrolled viral replication came from a quantitative
291 complementation test in which the $Irf3^{KO}$ allele was combined either with a CC071 or a B6
292 (functional) allele. Altogether, these results show that the *Irf3* defect in CC071 abrogates its
293 transcriptional activity. Unfortunately, none of the antibodies recognizing the N-terminal
294 protein domain that we tested worked in our hands in western blot. Therefore, we could not
295 establish whether the *Irf3* mRNA detected by RNAseq is translated into an abnormal protein
296 or not. However, the *in vivo* observation that $Irf3^{KO/71}$ and $Irf3^{71/71}$ backcross mice displayed
297 the same phenotypes upon ZIKV infection shows that the two alleles are functionally
298 equivalent in this context.
299 *Irf3* maps to a chromosomal region that CC071 inherited from CAST/EiJ, like the resistant
300 CC001 strain (and CC046/Unc, not available to us). The CC071-specific mutation may have
301 arisen during the inbreeding generations leading to this strain. Alternatively, the mutation
302 might have been segregating in the CAST/EiJ founders and transmitted by chance only to the
303 CC071 breeding funnel. Since all CAST/EiJ founders used in CC crosses originated from The

304 Jackson Laboratory colony, genotyping past and present breeders of this colony could not only
305 unravel the origin of the mutation but also allow eliminating this mutation to avoid unwanted
306 effects.
307 Notably, this is not the first example of a CC-strain-specific mutation. We (22) and others (23)
308 previously reported the extreme susceptibility of CC042/GeniUnc (CC042) to *Salmonella*
309 Typhimurium and to *Mycobacterium tuberculosis*, respectively, as a consequence of a *de novo*
310 15-nucleotide deletion in the *Itgal1* gene. In the case of *Salmonella* Typhimurium, CC042 was
311 standing out, with bacterial loads up to 1000 times higher than other CC and the susceptible
312 B6 strains. In our previous study on ZIKV, CC071 was the most susceptible strain, but its peak
313 viral load was just the highest in a continuous distribution of values. Additionally, this is not
314 the first example of a *Irf3* spontaneous variant identified in mice modulating susceptibility to
315 bacterial (24) or viral infections (25).
316 *Irf3* is an important transcription factor involved in the innate immune response. It is
317 constitutively expressed and, at rest, inactive IRF3 is present in the cytoplasm. Upon viral entry
318 (or other stimuli that activate TLRs such as TLR3 and 4 or RIG-I-like receptors), signal
319 transduction leads to the phosphorylation of IRF3, resulting in its dimerization and
320 translocation to the nucleus where it binds to the *Ifnb1* promoter (26). This mechanism leads
321 to the very fast production of IFNβ which is secreted by the cell and triggers the immediate
322 response to viral infection through the activation of ISGs with diverse antiviral functions (27).
323 In addition to its transcriptional activity, IRF3 has been shown to counter viral infection by two
324 additional mechanisms. IRF3 induces apoptosis through the RLR-induced IRF3-mediated
325 pathway of apoptosis (RIPA) in infected cells (28) and inhibits NF-κB-mediated inflammation
326 through the repression of IRF3-mediated NF-κB activity (RIKA) (29). These newly described
327 roles of IRF3 depend on other protein domains than those involved in its transcriptional

328 activity. Whether these activities are also abrogated by the CC071 *Irf3* mutation remains to be
329 established.
330 In mice, studies that used *Irf3*-deficient cellular models have consistently reported decreased
331 IFN-I production and/or increased viral replication. For example, after infection with WNV,
332 viral replication was increased in B6-*Irf3* KO bone marrow macrophages (BMMs) and
333 moderately in primary neurons (30). Higher viral replication was observed in herpes simplex
334 virus 1 (HSV-1)-infected B6-*Irf3* KO bone marrow-derived dendritic cells (BMDCs) and BMMs,
335 and IFNβ was reduced in BMDCs supernatants (31). Similarly, *Ifnb1* expression was reduced in
336 HSV-1-infected (32) and CHIKV-infected (33) B6-*Irf3* KO MEFs. In line with these findings, our
337 study provides, to our knowledge, the first evidence for a role of *Irf3* in the infection of murine
338 cells by ZIKV. Moreover, we recently reported that primary cultured neurons (PCNs) show a
339 delayed activation of the *Ifnb1* expression upon ZIKV exposure compared with MEFs, and that
340 this delay is even longer in PCNs derived from CC071 compared with CC001 (34). The
341 identification of the *Irf3* mutation in CC071 provides an explanation for this observation,
342 although it would require confirmation in B6-*Irf3* KO PCNs.
343 In contrast, *in vivo* studies have reported inconsistent consequences of *Irf3* deficiency
344 between viral infections. Here, we did not observe any differences in clinical signs nor in
345 plasma viral loads between B6 and B6-*Irf3* KO mice (pre-treated or not with the MAR1-5A3
346 antibody), consistently with a previous study that reported neither mortality, nor body weight
347 loss after ZIKV infection (10). Likewise, B6-*Irf3* KO mice have been reported to show no
348 mortality and low virus load in the circulation following dengue virus (35) and CHIKV infection
349 (33). Contrastingly, WNV infection was lethal in all B6-*Irf3* KO mice while 65% of infected WT
350 mice survived (30). Differences were also associated with the route of infection. For example,
351 all WT and B6-*Irf3* KO mice survived after intravenous inoculation with HSV-1 (32), while

352 intranasal inoculation led to 90% mortality in B6-*Irf3* KO but only 30% in WT mice (36).In
353 humans, LOF mutations in *Irf3* have been associated with increased susceptibility to diseases
354 caused by WNV (37,38), HSV-1 (39,40) and more recently by SARS-CoV-2 (41). Discrepancies
355 between the consequences of *Irf3* deficiency in *in vitro* and *in vivo* experiments likely reflect
356 differences between a single cell type model with an intrinsic capacity to mount a more or less
357 IRF3-dependent IFN-I response, and a multicellular organism in which the paracrine effect of
358 IFN-I produced by the most reactive cells induces protection of other, less reactive, cell types.
359 In fact, we have recently reported such cooperation between neurons and microglia cells (34).
360 Our *in vivo* data, showing high plasma viral loads and clinical signs in all CC071 and half of
361 backcross mice after MAR1-5A3 treatment, demonstrated that the high susceptibility of
362 CC071 mice requires the contribution of other recessive alleles. Since their effect was
363 observed in mice which IFNAR receptor had been blocked, we conclude that their mode of
364 action is not dependent on an intact IFN-I response. Moreover, the comparison between the
365 results of the complementation test on MEFs, with CC071 and *Irf3*$^{KO/71}$ yielding very similar
366 data, and the *in vivo* observation that CC071 showed higher viremia than *Irf3*$^{KO/71}$ F1 mice,
367 suggests that these other susceptibility alleles may not act at the cell level, at least during the
368 first 72 hpi, but rather at a more integrated or systemic level. Whether or not these alleles
369 require *Irf3* deficiency to induce the susceptibility observed in the CC071 mice has yet to be
370 determined. While our limited understanding of the severe disease developing in CC071 ZIKV-
371 infected mice does not point at potential mechanisms, identifying these alleles will allow
372 disentangling the genetic factors controlling ZIKV and other viruses' pathogenesis.
373
374

375 Material and methods
376

377 *Mice and crosses*

378 C57BL/6J (B6) mice were purchased from Charles River Laboratories France. Collaborative
379 Cross strains (CC001/Unc, CC071/TauUnc, CC005/TauUnc, CC011/Unc, CC026/GeniUnc,
380 CC061/GeniUnc, CC021/Unc, CC006/TauUnc, CC025/GeniUnc, CC039/Unc, CC060/Unc) were
381 purchased from the Systems Genetics Core Facility, University of North Carolina and bred at
382 the Institut Pasteur. *Irf3 Irf7* double KO mice (C57BL/6J-*Bcl2l12*/*Irf3*$^{tm1Ttg}$ *Irf7*$^{tm1Ttg}$,(32,42))
383 were bred at the Institut Pasteur and backcrossed to B6 mice to generate *Irf3* single KO mice
384 (B6-*Irf3* KO ). Genetic mapping was performed on MEFs derived from (CC001 x CC071) x CC071
385 and CC071 x (CC001 x CC071) backcross embryos. For the quantitative complementation test,
386 MEFs were derived from CC071, B6-*Irf3* KO and (B6-*Irf3*$^{+/KO}$ x CC071) embryos.. *In vivo*
387 experiments were performed on B6, B6-*Irf3* KO, CC071, (CC071 x *Irf3* KO) F1 and CC071 x
388 (CC071 x *Irf3* KO)backcross mice. All crosses are described as female x male. All mice were
389 maintained as described previously (15). Mouse experiments were approved by the Institut
390 Pasteur Ethics Committee and authorized by the French Ministry of Research (project #19469),
391 in compliance with French and European regulations.
392

393 *ZIKA virus*

394 The FG15 Asian Zika virus (ZIKV) strain, isolated from a patient during ZIKV outbreak in French
395 Guiana in December 2015, was obtained from the Virology Laboratory of the Institut Pasteur
396 of French Guiana. Viral stock (passage 5) was prepared from supernatant of infected C6/36
397 cells, clarified by centrifugation at 800g and titrated on Vero cells by focus-forming assay.
398

399 *Mouse infection*

400 All infection experiments were performed in a biosafety level 3 animal facility and mice were
401 kept in isolators. Six- to 10-week-old, male or female mice were injected intraperitoneally with
402 $10^7$ PFU of ZIKV FG15. In some *in vivo* experiments, mice received an IP injection of 2 mg of
403 MAR1-5A3 anti-IFNAR antibody (Euromedex, Cat#BX-BE0241) one day prior infection. Mouse
404 numbers are indicated in figure legends. Both males and females were used since no
405 differences between sexes were detected in our previous and present experiments. Clinical
406 signs and body weight loss were recorded for up to seven days post infection. Blood samples
407 were collected on EDTA from the retromandibular vein for plasma viral load assessment.
408 Quantification of ZIKV viral copies by qPCR was previously described (15).

409

410 *MEFs isolation*

411 Pregnant females were euthanized at day 13.5-15.5 of gestation. For B6, CC001, CC071 and
412 crosses used for genetic mapping and the complementation test, MEFs were isolated from
413 individual fetuses to obtain biological replicates. For other CC strains, MEFs were derived from
414 individual or pooled fetuses. Fetus bodies were chopped and digested with trypsin (Gibco
415 Cat#25300054), then cultured at 37°C and 5% $CO_2$ in complete medium (DMEM Gibco Cat#
416 31966047, 10% fetal bovine serum PAA Laboratories Cat#A15-101, 1% penicillin/streptomycin
417 Sigma Cat#P4333). MEFs were used until passage 2. For the backcross experiment, MEF lines
418 were isolated from 51 backcross fetuses. Heads were used to prepare DNA for whole-genome
419 genotyping.

420

421 *MEFs infection*

422 MEFs were seeded at $5.10^4$ cells per well in 24-well plates the day before infection. They were
423 exposed to ZIKV FG15 strain at a MOI of 5 for 2 hours after which the inoculum was replaced
424 with fresh complete medium and MEFs were incubated for up to 72 hours. For kinetics studies,
425 different wells were used for each time point. Backcross MEFs were infected in 6 infection
426 experiments, each of which included one CC001 and one CC071 MEF lines.
427
428 *MEFs IFNα stimulation*
429 MEFs were seeded at $5.10^4$ cells per well in 24-well plates one day before stimulation and
430 treated with 300 IU/mL IFNα (Miltenyi Biotec Cat#130-093-131) and incubated for up to 24
431 hours.
432
433 *Focus forming assay*
434 Quantification of ZIKV particles was performed by focus forming assay on Vero cells (ATCC
435 CRL-1586) as previously described (15).
436
437 *RNA extraction from cells*
438 MEFs were lysed in 350µL of RLT buffer (Qiagen) with 1% β-mercaptoethanol. RNA was
439 extracted using RNeasy Mini Kit (Qiagen Cat#74104) according to the manufacturer's
440 instructions, with addition of DNase I (Qiagen Cat# 79254) to prevent genomic DNA
441 contamination.
442
443 *Reverse transcription and qPCR*
444 Reverse-transcription was performed on 200ng of RNA using Superscript II polymerase
445 (Invitrogen Cat#18064022) and RNaseOUT ribonuclease inhibitor (Invitrogen Cat#10777019).

446 qPCR was performed on 20ng of cDNAs using Power SYBR Green PCR Master Mix (Applied
447 Biosystems Cat#4367659) and 6pmol of each primer, on a QuantStudio 12K Flex or a ViiA 7
448 (ThermoFisher Scientific). Primers (Eurofins) sequences are provided in Sup Table 1. Gene
449 expression was expressed on a Log10 scale of relative expression to the reference *Tbp* gene.
450
451 *Genotyping*
452 Genomic DNA was prepared from backcross fetuses' heads by proteinase K digestion, phenol-
453 chloroform extraction and ethanol precipitation according to standard protocols. Whole-
454 genome genotyping was performed at Neogen (Neogen/Geneseek, Inc, Lincoln, NE, USA)
455 using the MiniMUGA array containing 11,125 SNP markers. For the quantitative
456 complementation test, *Irf3* and *Irf7* genotyping was performed by Transnetyx (Cordova, TN)
457 by real-time PCR on fetuses' heads. (CC071 x *Irf3* KO) x CC071 backcross individuals were
458 genotyped by PCR using primers amplifying the intron 6 of $Irf3^{+}$ and $Irf3^{KO}$ but not $Irf3^{71}$ alleles.
459 Primers (Eurofins) sequences are provided in Sup Table 1.
460
461 *RNA splicing analysis from RNA sequencing data*
462 RNA sequencing data were produced as described in the Supplementary methods. Splicing
463 analysis of the *Irf3* gene was performed using Majiq 2.4 (43) with default parameters to
464 investigate alternative transcripts between genotypes.
465
466 *Immunofluorescence*
467 MEFs were plated on glass coverslips before infection, fixed with 4% paraformaldehyde for 20
468 min and permeabilized with 100% methanol for 10 min at -20°C. Cells were incubated with
469 blocking buffer (5% FBS 0.3% triton in PBS) for 1 hour, with primary antibodies diluted in

470 antibody incubation buffer (AIB: 1% BSA 0.3% triton in PBS) overnight at 4°C and with
471 secondary antibodies and Hoechst (dilution 1:1000) diluted in AIB for 1 hour. Coverslips were
472 mounted on slides and imaged with a widefield microscope (Zeiss Axio Observer.Z1 with a
473 Plan-Apochromat 20x/0.8 M27 objective and a Hamamatsu sCMOS ORCA-Flash 4.0 v3
474 camera). ZEN blue 2012 software (ZEISS) imaging software was used for image capture and
475 Image J software (National Institutes of Health) to adjust brightness and contrast. Primary and
476 secondary antibodies are indicated in Sup Table 2.
477
478 *Western blot*
479 MEFs were trypsinized for 5 min, washed and lysed in a protein extraction buffer (10mM
480 TrisHCl pH7.5, 5mM EDTA, 150mM NaCl, 30mM $Na_2HPO_4$, 50mM NaF, 10% glycerol, 1% NP40,
481 1X cOmplete (Roche #11873580001), 1X PhosSTOP (Roche #4906845001), 1/1000 benzonaze
482 (Sigma Cat#E1014)) for 30 min at 4°C. Proteins diluted in Laemmli were resolved on 4-12% Bis-
483 Tris gels (Invitrogen Cat#NP0323BOX) in MOPS buffer (Invitrogen Cat#NP0001) and
484 transferred to nitrocellulose membranes (Bio-Rad Cat#1620112) in a 25mM Tris 200mM
485 glycine 20% ethanol buffer. Blots were blocked in 5% milk in TBS-T (0.1% Tween20 in Tris Base
486 Sodium), incubated with primary antibodies diluted in 3% milk in TBST overnight at 4°C, and
487 incubated with secondary antibodies diluted in 3% milk in TBST for 90 min. Blots were revealed
488 with ECL substrate (Thermo Scientific Cat#32132) and imaged with X-ray films. Primary and
489 secondary antibodies are indicated in Sup Table 2.
490
491 *Statistical analysis*
492 Statistical analyses were performed using R version 4.1.0 (44). Viral titers, gene expression
493 and genome copies were log-transformed for graphs and statistical tests. One way ANOVA

494 followed by Tukey HSD were used for testing multiple comparisons. For *in vivo* studies without
495 MAR1-5A3 treatment, non-parametric Kruskal-Wallis followed by Wilcoxon tests with Holm
496 correction for multiple testing were used to handle values below the limit of detection. Linear
497 discriminant analysis (LDA) was conducted using the MASS package (45). The LDA was trained
498 on the phenotypes of the two parental CC001 and CC071 strains from each infection batch.
499 LDA coefficients were applied to backcross mice for assignment to "CC071-like" or "CC001-
500 like" groups.
501
502 *Genetic analysis*
503 Raw genotypes were curated using the stuart package (46). QTL mapping was performed using
504 R/qtl (47). LDA prediction was used as a binary trait. Statistical significance thresholds were
505 computed by data permutation (n=1000). 95% confidence interval was estimated using the
506 Bayesian method.

**Acknowledgements**

We thank Matthieu Prot, Maxime Chazal and Sandrine Vandormael-Pournin for technical advice and for providing reagents. We are grateful to Tommy Penel and Rachid Chennouf of the Institut Pasteur Central Animal Facility of the C2RA (Center for Animal Resources and Research) for the careful breeding of CC strains and for the maintenance of mice in the BSL-3 animal facility, respectively. We thank Etienne Simon-Loriere and Nolwenn Jouvenet for scientific advice and continuous support along this project.

**Author contributions**

X.M. conceived and supervised this study. M.B. and C.M. designed and performed the experiments and analyzed data. L.C. and C.R.P. performed experiments. E.K. analyzed RNAseq data. X.M. designed experiments and analyzed data. E.B. provided conceptual advice. M.B., C.M. and X.M. wrote the paper. All authors commented on and edited the manuscript.

**Funding**

This work was supported by grants from the Agence Nationale de la Recherche (ANR) NeuroZika (ANR-20-CE16-0017) and from the French Government's Investissement d'Avenir program, Laboratoire d'Excellence: IBEID (Integrative Biology of Emerging Infectious Diseases, ANR-10-LABX-62-IBEID). C.M. and M.B. were supported by doctoral fellowships from grant ANR-10-LABX-62-IBEID.

**Availability of data and materials**

530 RNAseq primary data are available from the European Nucleotide Archive (accession number
531 E-MTAB-12765). All other experimental data that support the finding of this study are
532 available from the corresponding authors upon reasonable request.
533
534 **Competing interests**
535 The authors declare that they have no competing interests.
536

537

538 **Figure legends**

539

540 **Figure 1. CC071 MEFs fail to control viral replication, with delayed *Ifnb1* expression but**
541 **normal response to IFN-I.** (A, B) MEFs derived from B6 (black circles), CC001 (blue triangles)
542 and CC071 (red squares) were infected with ZIKV at a MOI of 5 and analyzed 24, 48 and 72
543 hpi. (A) Viral titer in supernatants was quantified by FFA. (B) *Ifnb1* expression was normalized
544 to *Tbp* reference gene. Data are mean +/- sem from 3 to 4 biological replicates per strain (MEFs
545 derived from individual embryos). (C) MEFs were stimulated with recombinant IFNα. *Ifitm3*
546 relative expression normalized to *Tbp* reference gene is shown as an example of ISG. Data are
547 mean +/- sem from 2 to 3 biological replicates. Blue asterisks and black hashes show statistical
548 significance of CC071 compared to CC001 and to B6, respectively (ANOVA followed by Tukey
549 HSD, */# $p < 0.05$, **/## $p < 0.01$, ***/### $p < 0.001$).

550

551 **Figure 2. Haplotype analysis fails to identify a gene from the *Ifnb1* induction pathway**
552 **associated with uncontrolled viral replication.** (A) Identification of CC strains which carry the
553 same ancestral haplotype as CC071 at the genes involved in the pathway leading to *Ifnb1*
554 expression. Colored boxes indicate matched haplotypes between CC071 and other CC strains.
555 Letters and colors designate the eight CC founder strains. A: A/J (yellow); B: C57BL/6J; C:
556 129S1/SvImJ (pink); D: NOD/ShiLtJ; E: NZO/HILtJ (light blue); F: CAST/EiJ (green); G: PWK/PhJ
557 (red); H: WSB/EiJ (purple). Doubled letters (eg AA) indicate homozygous genotypes.
558 Heterozygous genotypes are indicated by the two corresponding letters (eg AD). (B) Kinetics
559 of viral titer in MEFs from CC071 and the 8 CC strains shown in (A). Experimental conditions
560 were as in Figure 1A. n: number of technical replicates for each strain. Data are mean +/- sem

561 from the technical replicates. Letters show statistical significance between CC071 and other
562 strains. (ANOVA followed by Tukey HSD, a: $p < 0.05$, b: $p < 0.01$, c: $p < 0.001$).
563
564 **Figure 3. Backcross MEFs display either a CC001-like or a CC071-like phenotype.** MEFs
565 derived from CC001 (blue triangles), CC071 (red squares) and backcross (gray circles) embryos
566 were infected with ZIKV at a MOI of 5. (A) Viral titer and (B) *Ifnb1* expression in ZIKV-infected
567 MEFs from 9 backcross embryos. Experimental conditions were as in Figure 1A-B. Red and
568 blue curves show the results for CC071 and CC001 MEFs, respectively, from the same infection
569 experiment. (C) Results of LDA on the backcross MEFs. LDA coefficients were calculated from
570 *Ifnb1* expression data in CC001 and CC071 infected MEFs, and applied to backcross MEFs. The
571 graph shows the probability of each BC MEF to belong to the "CC001-like" group, resulting in
572 two distinct populations shown in blue ("CC001-like") and in red ("CC071-like"). n: number of
573 BC MEFs assigned to each group.
574
575 **Figure 4. Genetic analysis of *Ifnb1* expression in backcross MEFs identifies a major**
576 **determinant mapping to the *Irf3* locus.** (A) Genome-wide linkage analysis of the LDA
577 classification of backcross MEFs performed with R/qtl. X-axis: genomic location. Y-axis: LOD
578 score of the phenotype-genotype association. Genome-wide significance thresholds ($P = 0.05$,
579 $P = 0.1$ and $P = 0.63$) were computed from 1000 data permutation. The chromosome 7 peak
580 has a LOD score of 9.138. (B) Schematic representation of CC001 and CC071 chromosome 7
581 haplotypes, from https://csbio.unc.edu/CCstatus/CCGenomes/. Colors represent the CC
582 ancestral haplotypes (same colors as in Figure 2A). Thick vertical black lines show the peak's
583 95% Bayesian confidence interval (25.9-31.3 cM, corresponding to 40.1-50.6 Mb). The red line
584 shows the position of *Irf3* gene.

585

586 **Figure 5. CC071 *Irf3* mRNAs show abnormal splicing, resulting in defective IRF3 protein.** (A)
587 Schematic representation of the exons of the *Irf3* gene with the number of reads spanning
588 successive exons in the CC001 and CC071 RNAseq data (one sample of each strain). The red
589 box between CC071's exons 6 and 7 depicts a novel exon resulting from abnormal splicing. (B)
590 Schematic representation of the IRF3 protein structural domains (exon 1 is untranslated). Exon
591 8 encodes the serine rich region containing the phosphorylation sites for IRF3 activation. (C)
592 Western blot using an anti-C-terminal IRF3 antibody from mock-infected and ZIKV-infected
593 B6, CC001 and CC071 MEFs at 2 hpi, showing the absence of full-length IRF3 in CC071 MEFs.
594 Vinculin was used as a loading control. (D) Immunofluorescence using an anti-phosphorylated
595 IRF3 (pIRF3, green) in ZIKV-infected B6, CC001 and CC071 MEFs at 24 hpi, showing the absence
596 of pIRF3 in the nucleus of CC071 MEFs upon infection. Red-labeled 4G2 antibody labels ZIKV-
597 infected cells. Cell nuclear DNA labeled by Hoechst (blue). Quantification of the number of
598 infected and pIRF3 positive cells is presented in the table. Proportions were established on
599 420, 428 and 551 cells for CC001, CC071 and B6, respectively.

600

601 **Figure 6. Quantitative complementation test confirms that *Irf3* LOF in CC071 is responsible**
602 **for uncontrolled viral replication and delayed *Ifnb1* expression.** (A) Mice heterozygous for an
603 inactivated *Irf3* allele (B6-*Irf3*$^{+/KO}$) were mated with CC071 mice to produce four types of
604 embryos from which MEFs were derived. The genetic background and *Irf3* genotype is shown
605 below each type of embryos. (B) Viral titer and (C) *Ifnb1* expression in ZIKV-infected MEFs.
606 Experimental conditions were as in Figure 1A-B. Data are mean +/- sem from 6 biological
607 replicates for CC071 and 3 for the other groups. The asterisks represent the results of ANOVA
608 test between all groups (* $p < 0.05$). Results of the Tukey HSD post-hoc are as follows. Viral

609 titer at 72h: CC071 vs *Irf3*$^{+/71}$ and vs *Irf3*$^{+/KO}$: $p < 0.001$. *Irf3*$^{KO/71}$ vs *Irf3*$^{+/71}$ and vs *Irf3*$^{+/KO}$: $p <$

610 0.01. *Irf3*$^{KO/KO}$ vs *Irf3*$^{+/71}$ and vs *Irf3*$^{+/KO}$: $p < 0.05$. *Ifnb1* expression at 24hpi: CC071 vs *Irf3*$^{+/71}$

611 and vs *Irf3*$^{+/KO}$, *Irf3*$^{KO/71}$ vs *Irf3*$^{+/71}$ and vs *Irf3*$^{+/KO}$, *Irf3*$^{KO/KO}$ vs *Irf3*$^{+/71}$ and vs *Irf3*$^{+/KO}$: $p < 0.001$.

612 *Ifnb1* expression at 48hpi: CC071 vs *Irf3*$^{+/71}$and vs *Irf3*$^{+/KO}$, *Irf3*$^{KO/71}$ vs *Irf3*$^{+/71}$ and vs *Irf3*$^{+/KO}$,

613 *Irf3*$^{KO/KO}$ vs *Irf3*$^{+/71}$ and vs *Irf3*$^{+/KO}$: $p < 0.01$.

614 **Figure 7. *Irf3* LOF is not sufficient to explain CC071 susceptibility to ZIKV infection *in vivo*.**

615 (A) B6, B6-*Irf3* KO and CC071 mice were infected IP with $10^7$ FFUs of ZIKV and monitored for 7

616 days, without prior IP injection of MAR1-5A3 IFNAR-blocking monoclonal antibody. Plasma

617 viral load was quantified at days 1 to 3 p.i. by RT-qPCR. The two lines of the group legend (X-

618 axis) indicate the genetic background of the mice and their genotype at the *Irf3* locus,

619 respectively. Each dot represents one mouse. Groups were compared by Kruskal-Wallis

620 followed by Wilcoxon test with Holm correction for multiple testing (* $p < 0.05$). (B) B6, B6-

621 *Irf3* KO, CC071, (CC071 x *Irf3* KO) F1 and (CC071 x *Irf3* KO) x CC071 BC mice were infected IP

622 with $10^7$ FFUs of ZIKV after IP injection of 2 mg of MAR1-5A3 IFNAR-blocking monoclonal

623 antibody 24 h before infection, and monitored for 7 days. The graph shows plasma viral loads

624 quantified at day 2 p.i. by RT-qPCR. The two lines of the group legend (X-axis) indicate the

625 genetic background of the mice and their genotype at the *Irf3* locus, respectively. BC mice are

626 separated into two groups depending on the genotype at the *Irf3* gene: homozygous for the

627 CC071 mutant allele (*Irf3*$^{71/71}$), or heterozygous for the CC071 and the KO alleles (*Irf3*$^{KO/71}$). *Irf3*

628 genotyping results are presented in Figure S5. Each dot represents one mouse. Groups were

629 compared by ANOVA followed by Tukey HSD (* $p < 0.05$, ** $p < 0.01$, *** $p < 0.001$). Below

630 the graph is shown the distribution of clinical scores at day 7 p.i. in the same groups of mice

631 as above (0, no symptoms; 1, slight hunched posture; 2, ruffled fur, hunched posture and/or

632 mild ataxia; 3: prostration, ataxia, partial paralysis).**Supplemental information**

633

634 **Legend to supplemental figures**

635

636 **Figure S1. *Ifna4* expression is delayed in ZIKV-infected CC071 MEFs.** MEFs derived from B6
637 (gray circles), CC001 (blue triangles) and CC071 (red squares) were infected with ZIKV at a MOI
638 of 5. *Ifna4* expression was determined by RT-qPCR on MEFs total RNA by normalizing to *Tbp*
639 housekeeping gene. Data are mean +/- sem from 3 biological replicates. For one CC001, one
640 B6 and one CC071 replicates at 0 hpi and one CC071 replicate at 24 hpi, gene expression was
641 below the limit of detection. Blue asterisks and black hashes show statistical significance of
642 CC071 compared to CC001 and to B6, respectively (ANOVA followed by post-hoc Tukey HSD,
643 */# $p < 0.05$, *** $p < 0.001$).

644

645 **Figure S2. Delayed IFN-I expression in CC071 MEFs results from a constitutive defect in the**
646 **transcription activation cascade.** MEFs were transfected with either (A) poly(I:C), which
647 activates both TLR and RIG-I pathways, or (B) 3p-hpRNA, a RIG-I agonist. *Ifnb1* expression was
648 determined as in Figure 1B. Data are mean +/- sem from 3 biological replicates for CC001 and
649 CC071 (2 at 4 hours) or 2 biological replicates for B6 (1 at 4 hours). Blue asterisks and black
650 hashes show statistical significance of CC071 compared to CC001 and to B6, respectively
651 (ANOVA followed by post-hoc Tukey HSD, */# $p < 0.05$).

652

653 **Figure S3**. **Expression of genes involved in the *Ifnb1* induction pathway in ZIKV-infected MEFs**
654 **of B6, CC001 and CC071 strains.** MEFs derived from B6 (black circles), CC001 (blue triangles)
655 and CC071 (red squares) were infected with ZIKV at a MOI of 5. mRNA expression levels were
656 measured by RNAseq in non-infected (NI) and ZIKV-infected MEFs. (A) Number of upregulated

genes per strain at 16, 24 and 32 hpi (log2 fold-change > 1, FDR = 0.05). (B-G) Genes constitutively expressed. (H-N) Genes which expression is induced by the IFN-I response (ISGs). Expression levels are shown on a logarithmic scale. For *Ifnb1* expression, null counts were transformed to 1. Data are mean +/- sem from 3 biological replicates. Blue asterisks and black hashes show statistical significance of CC071 compared to CC001 and to B6, respectively (ANOVA followed by post-hoc Tukey HSD, */# $p < 0.05$, **/## $p < 0.01$, ***/### $p < 0.001$).

**Figure S4. (CC001xCC071)F1 MEFs show normal induction of *Ifnb1*.** *Ifnb1* expression upon ZIKV infection in CC001, CC071 and (CC001xCC071)F1 MEFs determined as in Figure 1B. Data are mean +/- sem from 3 biological replicates. Blue asterisks and orange hashes show statistical significance of CC071 compared to CC001 and to F1, respectively (ANOVA followed by post-hoc Tukey HSD, **/## $p < 0.01$).

**Figure S5. Genotyping of (CC071 x Irf3 KO) x CC071 backcross individuals.** Backcross individuals were genotyped by PCR with primers amplifying the intro 6 of Irf3 (sequences in Sup Table 1). The $Irf3^{KO}$ allele results in a band at 877pb while the $Irf3^{71}$ allele results in no band. Individuals 1, 5, 11, 14, 15, 16, 17, 19, 21, 22 and 23 are $Irf3^{KO/71}$ and individuals 2, 6, 7, 8, 9, 10, 12, 13 and 24 are $Irf3^{71/71}$.

## References


1. Cao-Lormeau VM, Blake A, Mons S, Lastère S, Roche C, Vanhomwegen J, et al. Guillain-Barré Syndrome outbreak associated with Zika virus infection in French Polynesia: a case-control study. Lancet. 9 avr 2016;387(10027):1531-9.

2. Carod-Artal FJ. Neurological complications of Zika virus infection. Expert Review of Anti-infective Therapy. 4 mai 2018;16(5):399-410.

3. Oliveira Melo AS, Malinger G, Ximenes R, Szejnfeld PO, Alves Sampaio S, Bispo de Filippis AM. Zika virus intrauterine infection causes fetal brain abnormality and microcephaly: tip of the iceberg?: Physician Alert. Ultrasound Obstet Gynecol. janv 2016;47(1):6-7.

4. Paixao ES, Cardim LL, Costa MCN, Brickley EB, de Carvalho-Sauer RCO, Carmo EH, et al. Mortality from Congenital Zika Syndrome — Nationwide Cohort Study in Brazil. N Engl J Med. 24 févr 2022;386(8):757-67.

5. Rossi SL, Ebel GD, Shan C, Shi PY, Vasilakis N. Did Zika Virus Mutate to Cause Severe Outbreaks? Trends in Microbiology. 1 oct 2018;26(10):877-85.

6. Liu ZY, Shi WF, Qin CF. The evolution of Zika virus from Asia to the Americas. Nat Rev Microbiol. mars 2019;17(3):131-9.

7. Manet C, Roth C, Tawfik A, Cantaert T, Sakuntabhai A, Montagutelli X. Host genetic control of mosquito-borne Flavivirus infections. Mamm Genome. 2018;29(7-8):384-407.

8. Rasmussen AL, Okumura A, Ferris MT, Green R, Feldmann F, Kelly SM, et al. Host genetic diversity enables Ebola hemorrhagic fever pathogenesis and resistance. Science. 21 nov 2014;346(6212):987-91.

9. Gralinski LE, Menachery VD, Morgan AP, Totura AL, Beall A, Kocher J, et al. Allelic Variation in the Toll-Like Receptor Adaptor Protein Ticam2 Contributes to SARS-Coronavirus Pathogenesis in Mice. G3 (Bethesda). 7 juin 2017;7(6):1653-63.

10. Lazear HM, Govero J, Smith AM, Platt DJ, Fernandez E, Miner JJ, et al. A Mouse Model of Zika Virus Pathogenesis. Cell Host Microbe. 11 mai 2016;19(5):720-30.

11. Grant A, Ponia SS, Tripathi S, Balasubramaniam V, Miorin L, Sourisseau M, et al. Zika Virus Targets Human STAT2 to Inhibit Type I Interferon Signaling. Cell Host & Microbe. juin 2016;19(6):882-90.

12. Sheehan KCF, Lai KS, Dunn GP, Bruce AT, Diamond MS, Heutel JD, et al. Blocking Monoclonal Antibodies Specific for Mouse IFN- *α* / *β* Receptor Subunit 1 (IFNAR-1) from Mice Immunized by *In Vivo* Hydrodynamic Transfection. Journal of Interferon & Cytokine Research. nov 2006;26(11):804-19.

13. Roberts A, Pardo-Manuel de Villena F, Wang W, McMillan L, Threadgill DW. The polymorphism architecture of mouse genetic resources elucidated using genome-

wide resequencing data: implications for QTL discovery and systems genetics. Mamm Genome. juill 2007;18(6-7):473-81.

14. Keane TM, Goodstadt L, Danecek P, White MA, Wong K, Yalcin B, et al. Mouse genomic variation and its effect on phenotypes and gene regulation. Nature. sept 2011;477(7364):289-94.

15. Manet C, Simon-Lorière E, Jouvion G, Hardy D, Prot M, Conquet L, et al. Genetic Diversity of Collaborative Cross Mice Controls Viral Replication, Clinical Severity, and Brain Pathology Induced by Zika Virus Infection, Independently of Oas1b. J Virol [Internet]. 17 janv 2020;94(3). Disponible sur: https://journals.asm.org/doi/10.1128/JVI.01034-19

16. Jasperse BA, Mattocks MD, Noll KM, Ferris MT, Heise MT, Lazear HM. Neuroinvasive flavivirus pathogenesis is restricted by host genetic factors in Collaborative Cross mice, independently of Oas1b [Internet]. bioRxiv; 2022 [cité 26 oct 2022]. Disponible sur: https://www.biorxiv.org/content/10.1101/2022.10.24.513634v1

17. Cartwright HN, Barbeau DJ, Doyle JD, Klein E, Heise MT, Ferris MT, et al. Genetic diversity of collaborative cross mice enables identification of novel rift valley fever virus encephalitis model. PLOS Pathogens. 14 juill 2022;18(7):e1010649.

18. McCartney S, Vermi W, Gilfillan S, Cella M, Murphy TL, Schreiber RD, et al. Distinct and complementary functions of MDA5 and TLR3 in poly(I:C)-mediated activation of mouse NK cells. Journal of Experimental Medicine. 21 déc 2009;206(13):2967-76.

19. Collaborative Cross Consortium. The Genome Architecture of the Collaborative Cross Mouse Genetic Reference Population. Genetics. 1 févr 2012;190(2):389-401.

20. Srivastava A, Morgan AP, Najarian ML, Sarsani VK, Sigmon JS, Shorter JR, et al. Genomes of the Mouse Collaborative Cross. Genetics. 1 juin 2017;206(2):537-56.

21. Brown AJ, Won JJ, Wolfisberg R, Fahnøe U, Catanzaro N, West A, et al. Host genetic variation guides hepacivirus clearance, chronicity, and liver fibrosis in mice [Internet]. Microbiology; 2023 mars [cité 24 mars 2023]. Disponible sur: http://biorxiv.org/lookup/doi/10.1101/2023.03.18.533278

22. Zhang J, Teh M, Kim J, Eva MM, Cayrol R, Meade R, et al. A Loss-of-Function Mutation in the Integrin Alpha L (Itgal) Gene Contributes to Susceptibility to Salmonella enterica Serovar Typhimurium Infection in Collaborative Cross Strain CC042. Infect Immun. 17 2019;88(1).

23. Smith CM, Proulx MK, Lai R, Kiritsy MC, Bell TA, Hock P, et al. Functionally Overlapping Variants Control Tuberculosis Susceptibility in Collaborative Cross Mice. Vance R, éditeur. mBio. 24 déc 2019;10(6):e02791-19.

24. Garifulin O, Qi Z, Shen H, Patnala S, Green MR, Boyartchuk V. Irf3 Polymorphism Alters Induction of Interferon Beta in Response to Listeria monocytogenes Infection. PLOS Genetics. 7 sept 2007;3(9):e152.

25. Moore TC, Al-Salleeh FM, Brown DM, Petro TM. IRF3 polymorphisms induce different innate anti-Theiler's virus immune responses in RAW264.7 macrophages. Virology. sept 2011;418(1):40-8.

26. Bourdon M, Manet C, Montagutelli X. Host genetic susceptibility to viral infections: the role of type I interferon induction. Genes Immun. déc 2020;21(6-8):365-79.

27. Schoggins JW. Interferon-Stimulated Genes: What Do They All Do? Annu Rev Virol. 29 sept 2019;6(1):567-84.

28. Chattopadhyay S, Kuzmanovic T, Zhang Y, Wetzel JL, Sen GC. Ubiquitination of the Transcription Factor IRF-3 Activates RIPA, the Apoptotic Pathway that Protects Mice from Viral Pathogenesis. Immunity. 17 mai 2016;44(5):1151-61.

29. Popli S, Chakravarty S, Fan S, Glanz A, Aras S, Nagy LE, et al. IRF3 inhibits nuclear translocation of NF-κB to prevent viral inflammation. Proc Natl Acad Sci USA. 13 sept 2022;119(37):e2121385119.

30. Daffis S, Samuel MA, Keller BC, Gale M Jr, Diamond MS. Cell-specific IRF-3 responses protect against West Nile virus infection by interferon-dependent and -independent mechanisms. PLoS Pathog. 27 juill 2007;3(7):e106.

31. Menachery VD, Leib DA. Control of Herpes Simplex Virus Replication Is Mediated through an Interferon Regulatory Factor 3-Dependent Pathway. J Virol. déc 2009;83(23):12399-406.

32. Honda K, Yanai H, Negishi H, Asagiri M, Sato M, Mizutani T, et al. IRF-7 is the master regulator of type-I interferon-dependent immune responses. Nature. 7 avr 2005;434(7034):772-7.

33. Schilte C, Buckwalter MR, Laird ME, Diamond MS, Schwartz O, Albert ML. Cutting Edge: Independent Roles for IRF-3 and IRF-7 in Hematopoietic and Nonhematopoietic Cells during Host Response to Chikungunya Infection. JI. 1 avr 2012;188(7):2967-71.

34. Manet C, Mansuroglu Z, Conquet L, Bortolin V, Comptdaer T, Segrt H, et al. Zika virus infection of mature neurons from immunocompetent mice generates a disease-associated microglia and a tauopathy-like phenotype in link with a delayed interferon beta response. J Neuroinflammation. 20 déc 2022;19(1):307.

35. Chen HW, King K, Tu J, Sanchez M, Luster AD, Shresta S. The roles of IRF-3 and IRF-7 in innate antiviral immunity against dengue virus. J Immunol. 15 oct 2013;191(8):4194-201.

36. Canivet C, Rhéaume C, Lebel M, Piret J, Gosselin J, Boivin G. Both IRF3 and especially IRF7 play a key role to orchestrate an effective cerebral inflammatory response in a mouse model of herpes simplex virus encephalitis. J Neurovirol. déc 2018;24(6):761-8.

37. Bigham AW, Buckingham KJ, Husain S, Emond MJ, Bofferding KM, Gildersleeve H, et al. Host genetic risk factors for West Nile virus infection and disease progression. PLoS One. 2011;6(9):e24745.

38. Cahill ME, Conley S, DeWan AT, Montgomery RR. Identification of genetic variants associated with dengue or West Nile virus disease: a systematic review and meta-analysis. BMC Infect Dis. déc 2018;18(1):282.

39. Mork N, Kofod-Olsen E, Sorensen KB, Bach E, Orntoft TF, Ostergaard L, et al. Mutations in the TLR3 signaling pathway and beyond in adult patients with herpes simplex encephalitis. Genes Immun. déc 2015;16(8):552-66.

40. Andersen LL, Mork N, Reinert LS, Kofod-Olsen E, Narita R, Jorgensen SE, et al. Functional IRF3 deficiency in a patient with herpes simplex encephalitis. J Exp Med. 24 août 2015;212(9):1371-9.

41. Zhang Q, Bastard P, Liu Z, Le Pen J, Moncada-Velez M, Chen J, et al. Inborn errors of type I IFN immunity in patients with life-threatening COVID-19. Science [Internet]. 24 sept 2020; Disponible sur: https://www.ncbi.nlm.nih.gov/pubmed/32972995 https://science.sciencemag.org/content/sci/370/6515/eabd4570.full.pdf

42. Sato M, Suemori H, Hata N, Asagiri M, Ogasawara K, Nakao K, et al. Distinct and essential roles of transcription factors IRF-3 and IRF-7 in response to viruses for IFN-alpha/beta gene induction. Immunity. oct 2000;13(4):539-48.

43. Vaquero-Garcia J, Barrera A, Gazzara MR, González-Vallinas J, Lahens NF, Hogenesch JB, et al. A new view of transcriptome complexity and regulation through the lens of local splicing variations. eLife. 1 févr 2016;5:e11752.

44. R Core Team. R: A Language and Environment for Statistical Computing [Internet]. 2021. Disponible sur: https://www.R-project.org/

45. Venables WN, Ripley BD. Modern Applied Statistics with S. Fourth Edition [Internet]. Fourth. Springer; 2002. Disponible sur: https://www.stats.ox.ac.uk/pub/MASS4/

46. Bourdon M, Montagutelli X. stuart: an R package for the curation of SNP genotypes from experimental crosses. G3 (Bethesda). 24 août 2022;jkac219.

47. Broman KW, Wu H, Sen S, Churchill GA. R/qtl: QTL mapping in experimental crosses. Bioinformatics. 1 mai 2003;19(7):889-90.

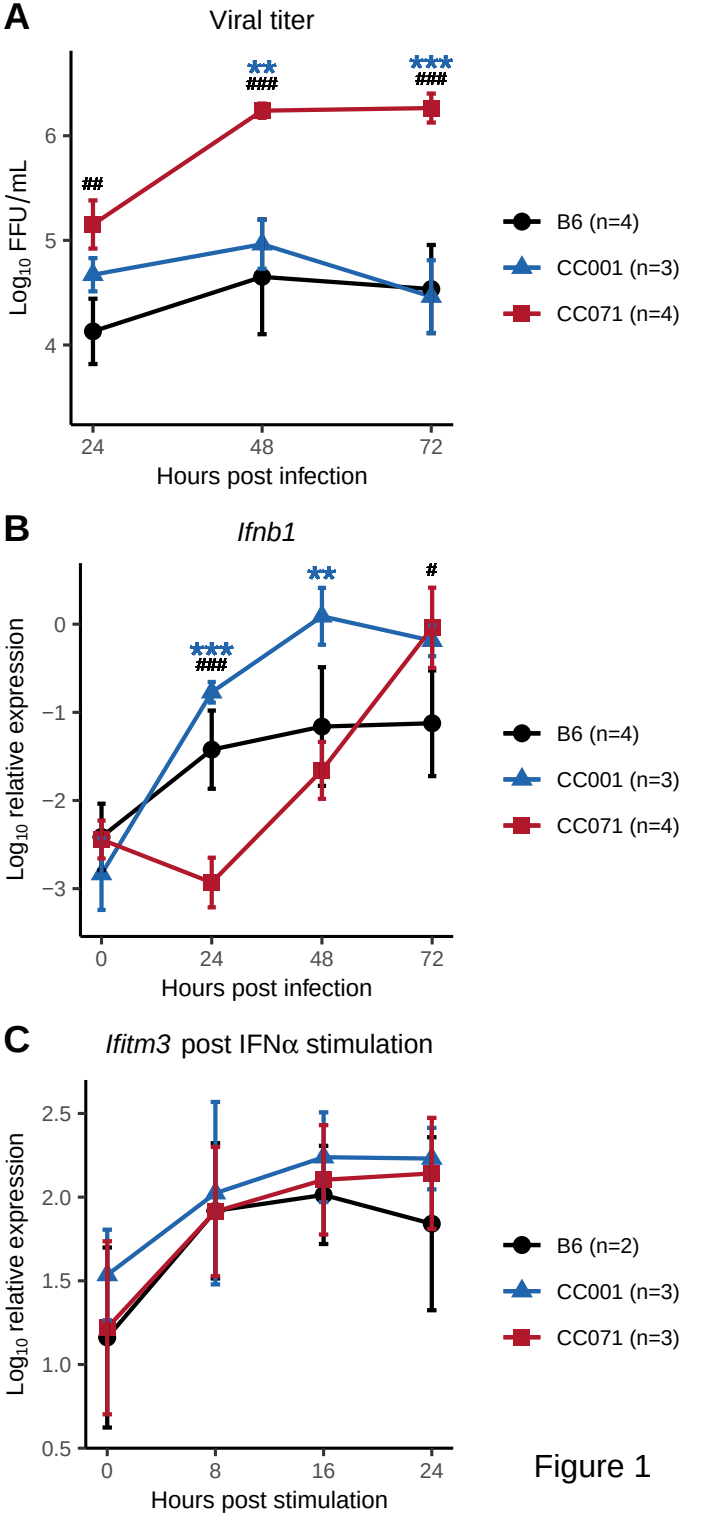
A
Viral titer
Log10 FFU/mL
6
5
4
24
48
72
Hours post infection
**
###
***
###
##
B6 (n=4)
CC001 (n=3)
CC071 (n=4)
B
Ifnb1
Log10 relative expression
0
−1
−2
−3
0
24
48
72
Hours post infection
***
###
**
#
B6 (n=4)
CC001 (n=3)
CC071 (n=4)
C
Ifitm3 post IFNα stimulation
Log10 relative expression
2.5
2.0
1.5
1.0
0.5
0
8
16
24
Hours post stimulation
B6 (n=2)
CC001 (n=3)
CC071 (n=3)

Figure 1

**A**

CC strains haplotypes

| Gene | Protein | CC071 | CC001 | CC005 | CC026 | CC021 | CC006 | CC025 | CC039 | CC060 |
|---|---|---|---|---|---|---|---|---|---|---|
| *Ddx58* | RIG−I | HH | BB | EE | CC | HH | AA | HH | AD | EE |
| *Ifih1* | LGP2 | GG | AA | DD | HH | GG | BB | AA | BB | CC |
| *Dhx58* | MDA−5 | FF | EE | DD | HH | FF | DD | FF | FF | EE |
| *Tlr3* | TLR3 | AA | AA | BB | CC | EE | AA | BB | FF | CC |
| *Mavs* | MAVS | CC | AA | DD | HH | GG | CC | DD | HH | DD |
| *Ticam1* | TRIF | CC | AA | EE | BB | CC | DD | HH | AA | EE |
| *Azi2* | NAP1 | EE | DD | FF | BB | FF | EE | GG | CC | EE |
| *Traf3* | TRAF3 | HH | HH | GG | CC | FF | CC | CC | AA | BB |
| *Tbk1* | TBK1 | HH | DD | GG | HH | AA | FF | AA | GG | BB |
| *Ikbke* | IKKε | CC | EE | CC | AA | EE | CC | CC | GH | AA |
| *Irf3* | IRF3 | FF | FF | HH | BB | CC | DD | EE | HH | BB |
| *Irf7* | IRF7 | HH | BB | DD | DD | HH | EE | DD | HH | DD |
| *Ifnb1* | IFNβ | HH | EE | DD | CC | HH | BB | HH | CC | DE |

**B**

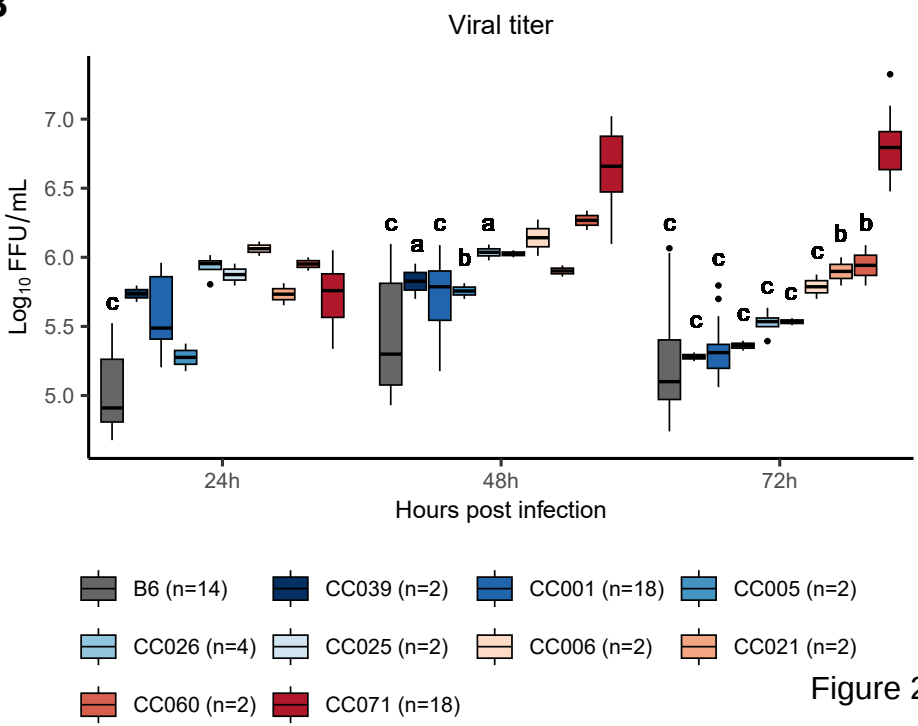


Figure 2

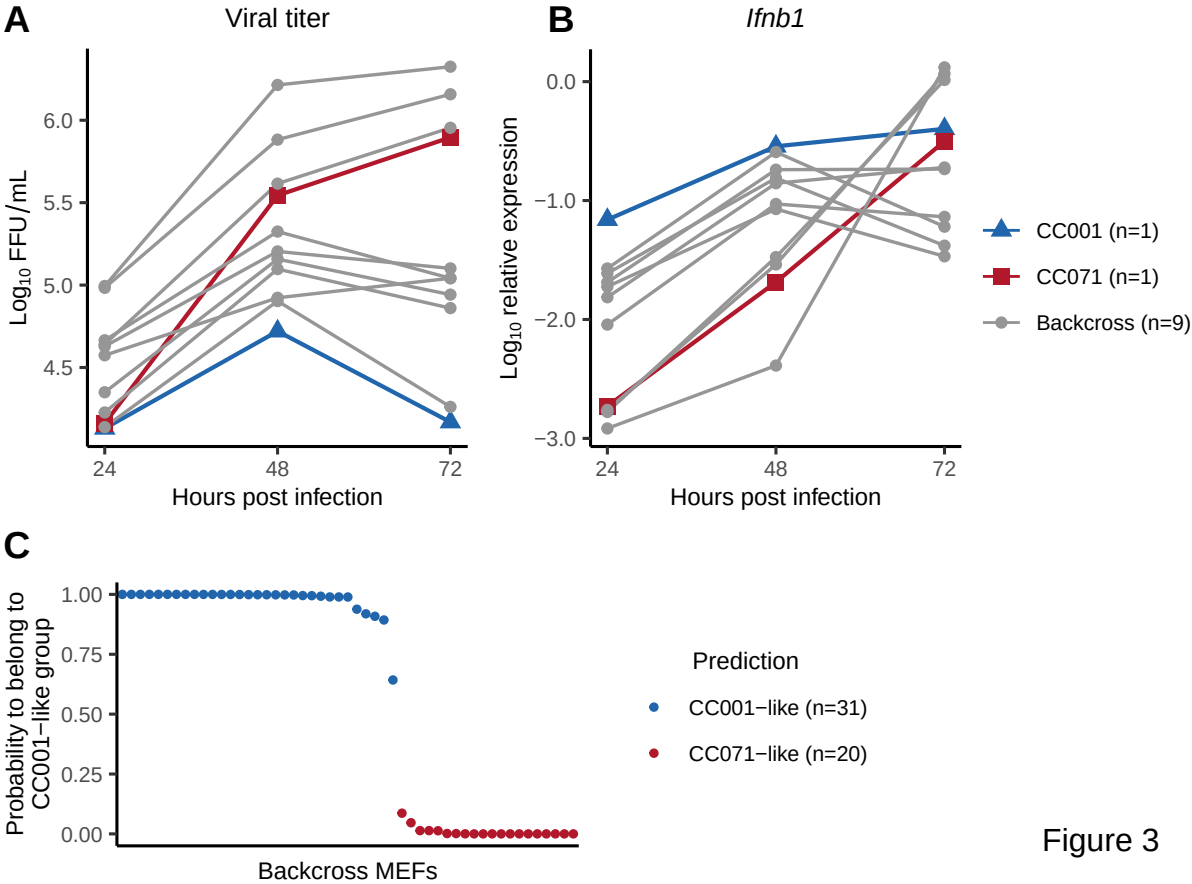
A
Viral titer
Log10 FFU/mL
6.0
5.5
5.0
4.5
24
48
72
Hours post infection
B
Ifnb1
Log10 relative expression
0.0
−1.0
−2.0
−3.0
24
48
72
Hours post infection
CC001 (n=1)
CC071 (n=1)
Backcross (n=9)
C
Probability to belong to CC001−like group
1.00
0.75
0.50
0.25
0.00
Backcross MEFs
Prediction
CC001−like (n=31)
CC071−like (n=20)

Figure 3

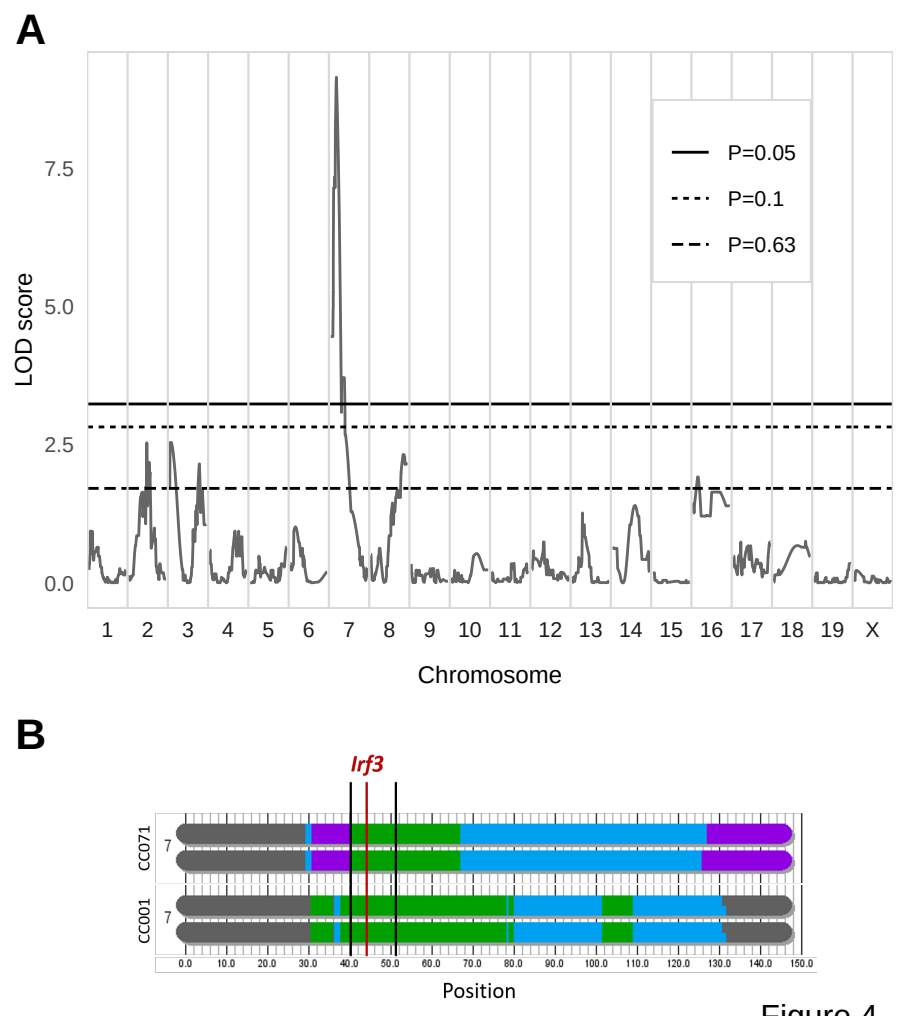
A
LOD score
7.5
5.0
2.5
0.0
P=0.05
P=0.1
P=0.63
1 2 3 4 5 6 7 8 9 10 11 12 13 14 15 16 17 18 19 X
Chromosome
B
Irf3
CC071
7
CC001
7
0.0 10.0 20.0 30.0 40.0 50.0 60.0 70.0 80.0 90.0 100.0 110.0 120.0 130.0 140.0 150.0
Position

Figure 4

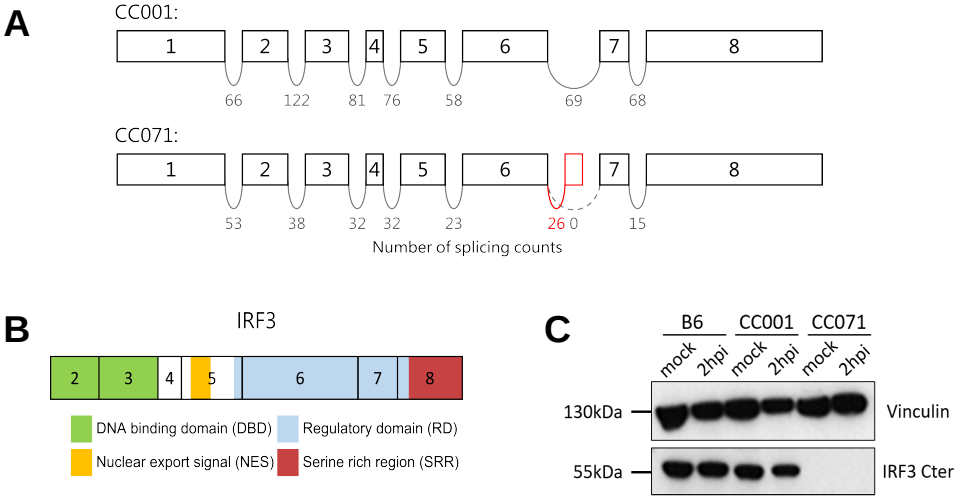


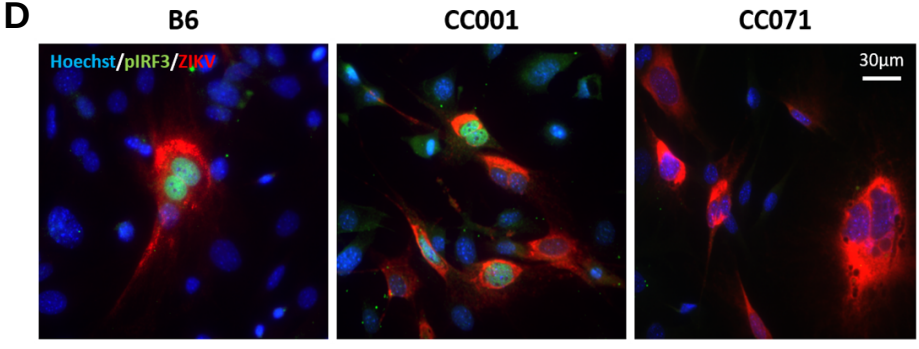


| Count | B6 | CC001 | CC071 |
|---|---|---|---|
| Infected cells | 24 | 91 | 76 |
| pIRF3 positive cells | 5 | 28 | 0 |
| **Percentage** | 21% | 31% | 0% |

Figure 5

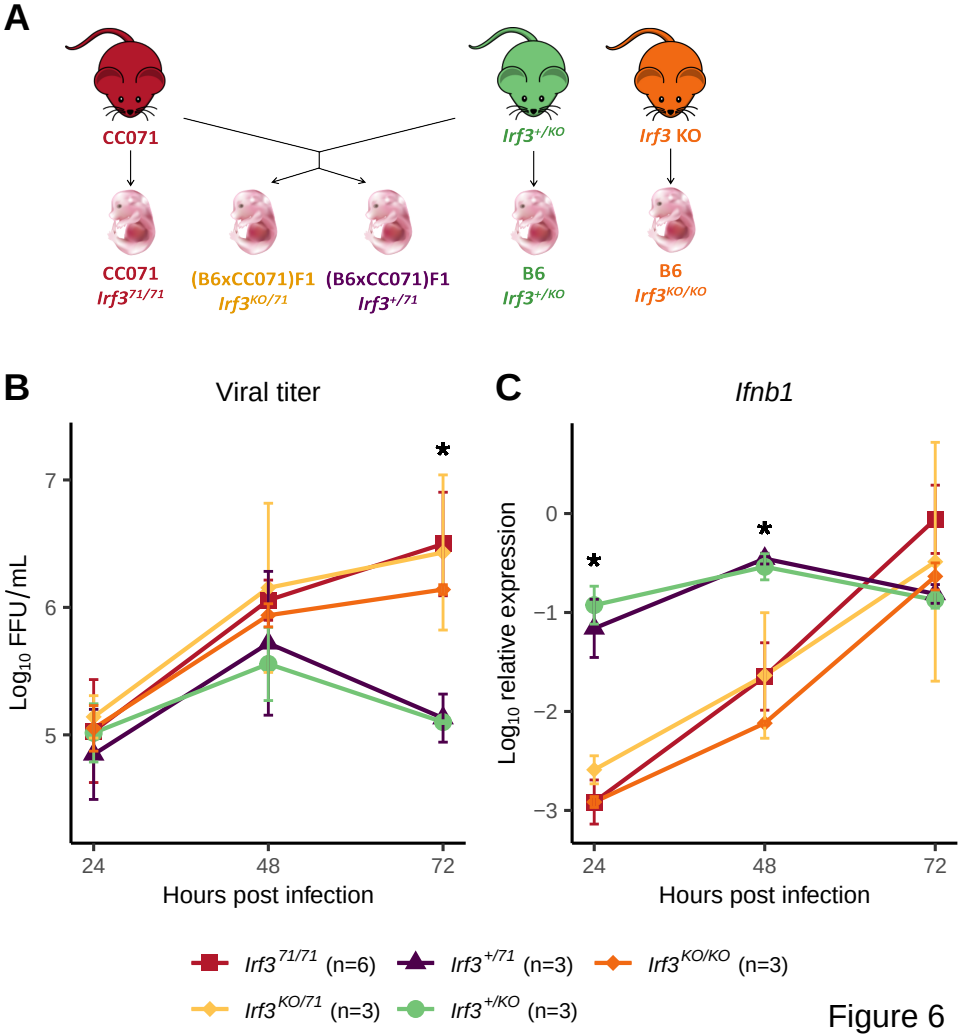
A
CC071
Irf3+/KO
Irf3 KO
CC071
Irf3 71/71
(B6xCC071)F1
Irf3 KO/71
(B6xCC071)F1
Irf3 +/71
B6
Irf3 +/KO
B6
Irf3 KO/KO
B
Viral titer
Log10 FFU/mL
7
6
5
24
48
72
Hours post infection
*
C
Ifnb1
Log10 relative expression
0
−1
−2
−3
24
48
72
Hours post infection
*
*
Irf3 71/71 (n=6)
Irf3 +/71 (n=3)
Irf3 KO/KO (n=3)
Irf3 KO/71 (n=3)
Irf3 +/KO (n=3)

Figure 6

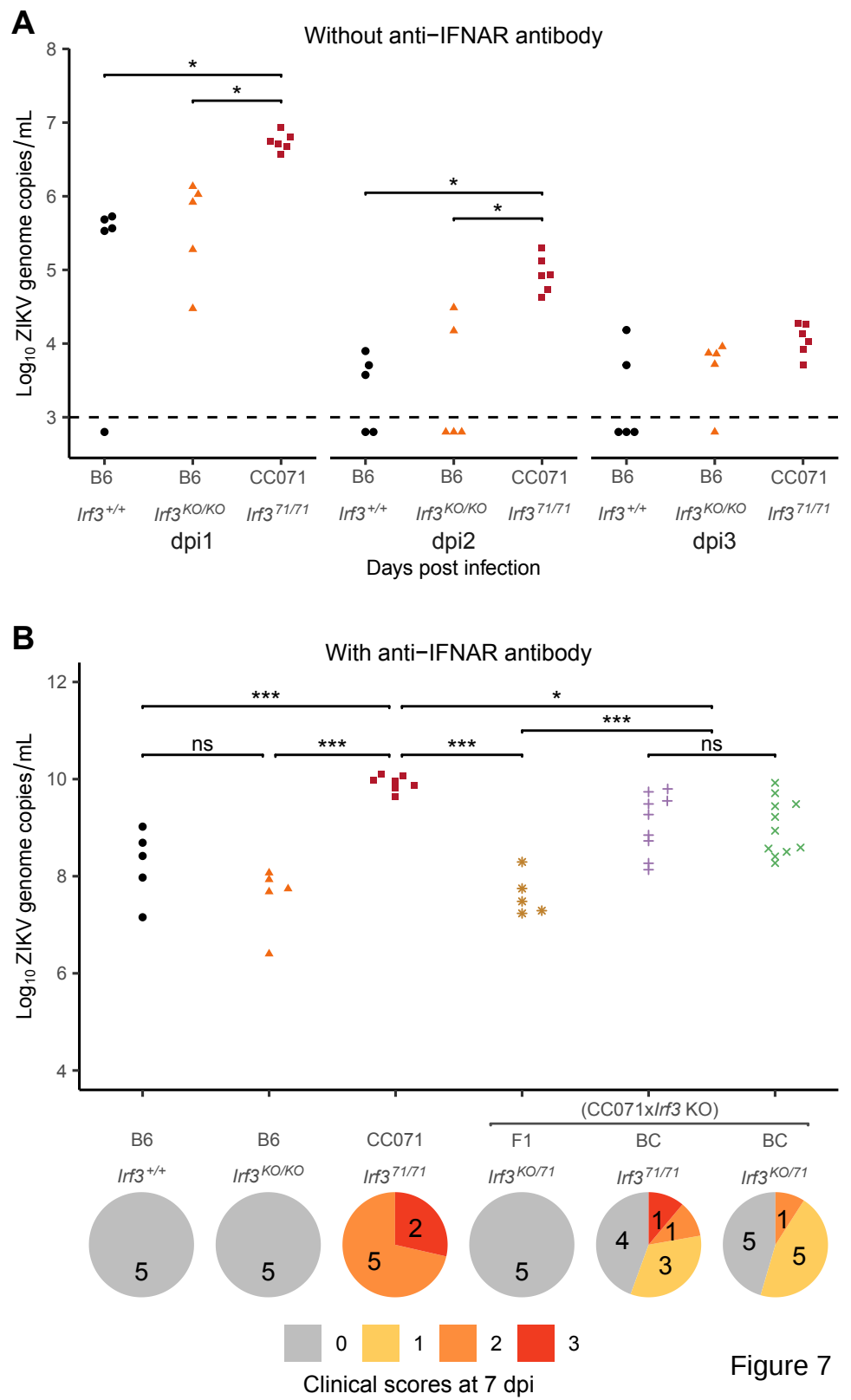
A
Without anti−IFNAR antibody
Log10 ZIKV genome copies/mL
8
7
6
5
4
3
*
*
*
*
B6
B6
CC071
B6
B6
CC071
B6
B6
CC071
Irf3+/+
Irf3KO/KO
Irf3 71/71
Irf3+/+
Irf3KO/KO
Irf3 71/71
Irf3+/+
Irf3KO/KO
Irf3 71/71
dpi1
dpi2
dpi3
Days post infection
B
With anti−IFNAR antibody
Log10 ZIKV genome copies/mL
12
10
8
6
4
***
*
***
ns
***
***
ns
(CC071xIrf3 KO)
B6
B6
CC071
F1
BC
BC
Irf3+/+
Irf3KO/KO
Irf3 71/71
Irf3KO/71
Irf3 71/71
Irf3KO/71
5
5
5
2
5
4
1
1
3
5
1
5
0
1
2
3
Clinical scores at 7 dpi

Figure 7

**Supplementary methods**

*MEFs stimulation with poly(I :C) and 3p-hpRNA*

For intracellular stimulation with Poly(I:C) or with 3p-hpRNA, MEFs were seeded at $1.10^5$ cells per well in 12-well plates the day before stimulation, transfected with 1 µg/mL Poly(I:C) (InvivoGen Cat#vac-pic) or 0.5 µg/mL 3p-hpRNA (InvivoGen Cat#tlrl-hprna) using 5 µL Lipofectamine LTX and 1 µL for poly(I:C) stimulation or 0.5 µL for 3p-hpRNA stimulation of Plus Reagent (ThermoFischer Scientific Cat#15338100), according to the manufacturer's instructions. After stimulation, MEFs were incubated for 8 to 24 hours.

*RNA sequencing*

MEF RNA was prepared as described in the main text. RNA integrity and quantification were assessed using the RNA Nano 6000 Assay Kit of the Bioanalyzer 2100 system (Agilent Technologies, CA, USA). One microgram of high-quality RNA samples (RIN > 9.2) representing biological triplicates were submitted to Novogene for RNA-sequencing (Novogene Beijing, China). Poly-A selected RNA was used for paired-end library preparation and transcriptome sequencing. Sequencing libraries were generated using NEBNext® UltraTM RNA Library Prep Kit for Illumina® (NEB, USA) following manufacturer's instructions. The library preparations were sequenced on an Illumina platform and paired-end reads were generated. The RNA-seq analysis was performed with Sequana 0.9.8 (1). In particular, we used the RNA-seq pipeline https://github.com/sequana/sequana_rnaseq) built on top of Snakemake 6.1.1 (2). Briefly, reads were trimmed from adapters using Cutadapt 2.7 then mapped to the *Mus musculus* genome assembly GCA_000001635.8 from NCBI using STAR 2.7.3a (3). FeatureCounts 1.6.4 (4) was used to produce the count matrix, assigning reads to features using corresponding annotation v92 from NCBI with strand-specificity information. Quality control statistics were summarized using MultiQC 1.6 (5). Clustering of transcriptomic profiles were controlled using Principal Component Analysis (PCA). Differential expression testing was conducted using DESeq2 library 1.24.0 (6) scripts indicating the significance (Benjamini-Hochberg adjusted p-values, false discovery rate FDR < 0.05) and the effect size (fold-change) for each comparison.

1. Cokelaer T, Desvillechabrol D, Legendre R, Cardon M. 2017. “Sequana”: a Set of Snakemake NGS pipelines. JOSS 2:352.

2. Köster J, Rahmann S. 2012. Snakemake—a scalable bioinformatics workflow engine. Bioinformatics 28:2520–2522.

3. Dobin A, Davis CA, Schlesinger F, Drenkow J, Zaleski C, Jha S, Batut P, Chaisson M, Gingeras TR. 2013. STAR: ultrafast universal RNA-seq aligner. Bioinformatics 29:15–21.

4. Liao Y, Smyth GK, Shi W. 2014. featureCounts: an efficient general purpose program for assigning sequence reads to genomic features. Bioinformatics 30:923–930.

5. Ewels P, Magnusson M, Lundin S, Käller M. 2016. MultiQC: summarize analysis results for multiple tools and samples in a single report. Bioinformatics 32:3047–3048.

6. Love MI, Huber W, Anders S. 2014. Moderated estimation of fold change and dispersion for RNA-seq data with DESeq2. Genome Biol 15:550.

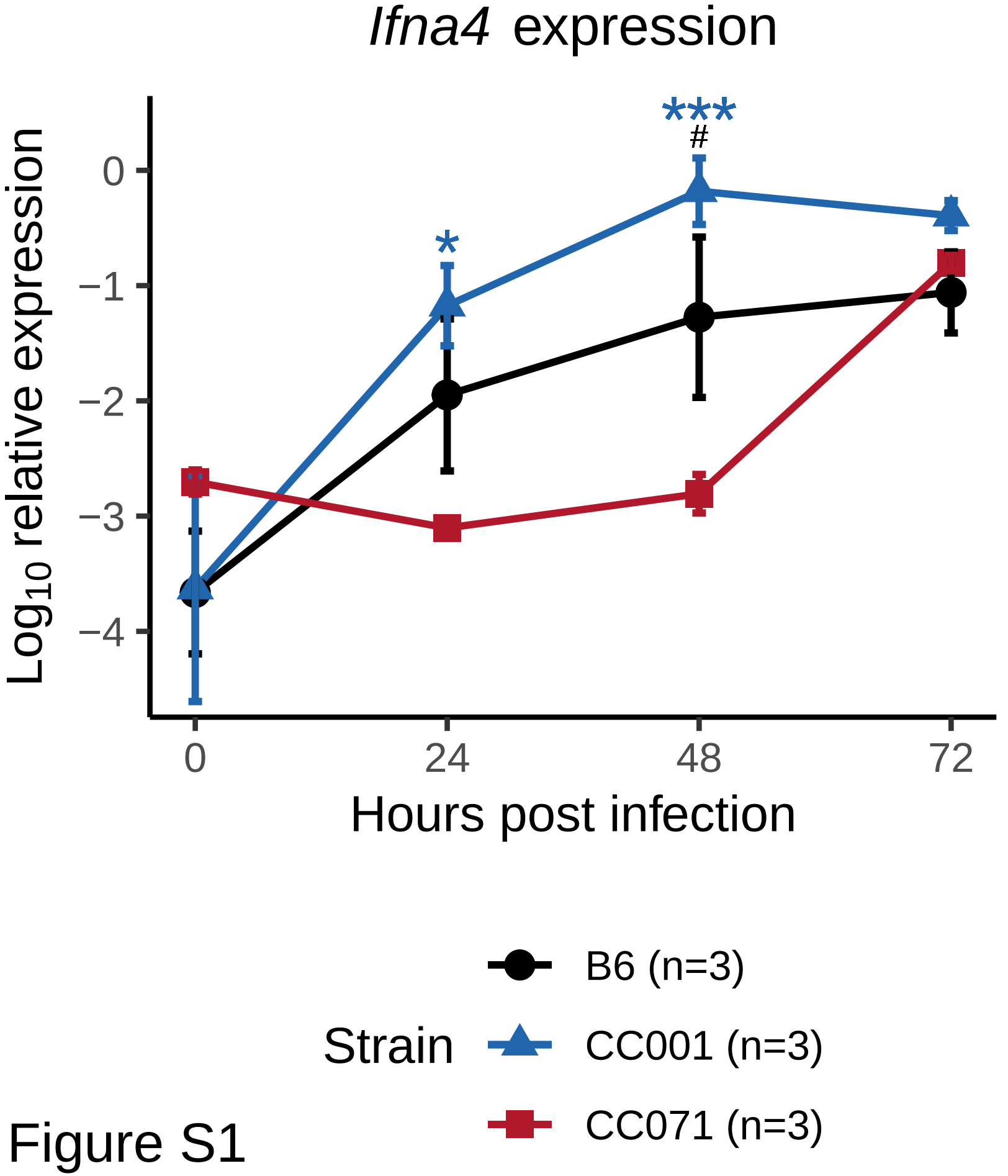
*Ifna4* expression
***
#
*
0
−1
−2
−3
−4
Log10 relative expression
0
24
48
72
Hours post infection
Strain
B6 (n=3)
CC001 (n=3)
CC071 (n=3)

Figure S1

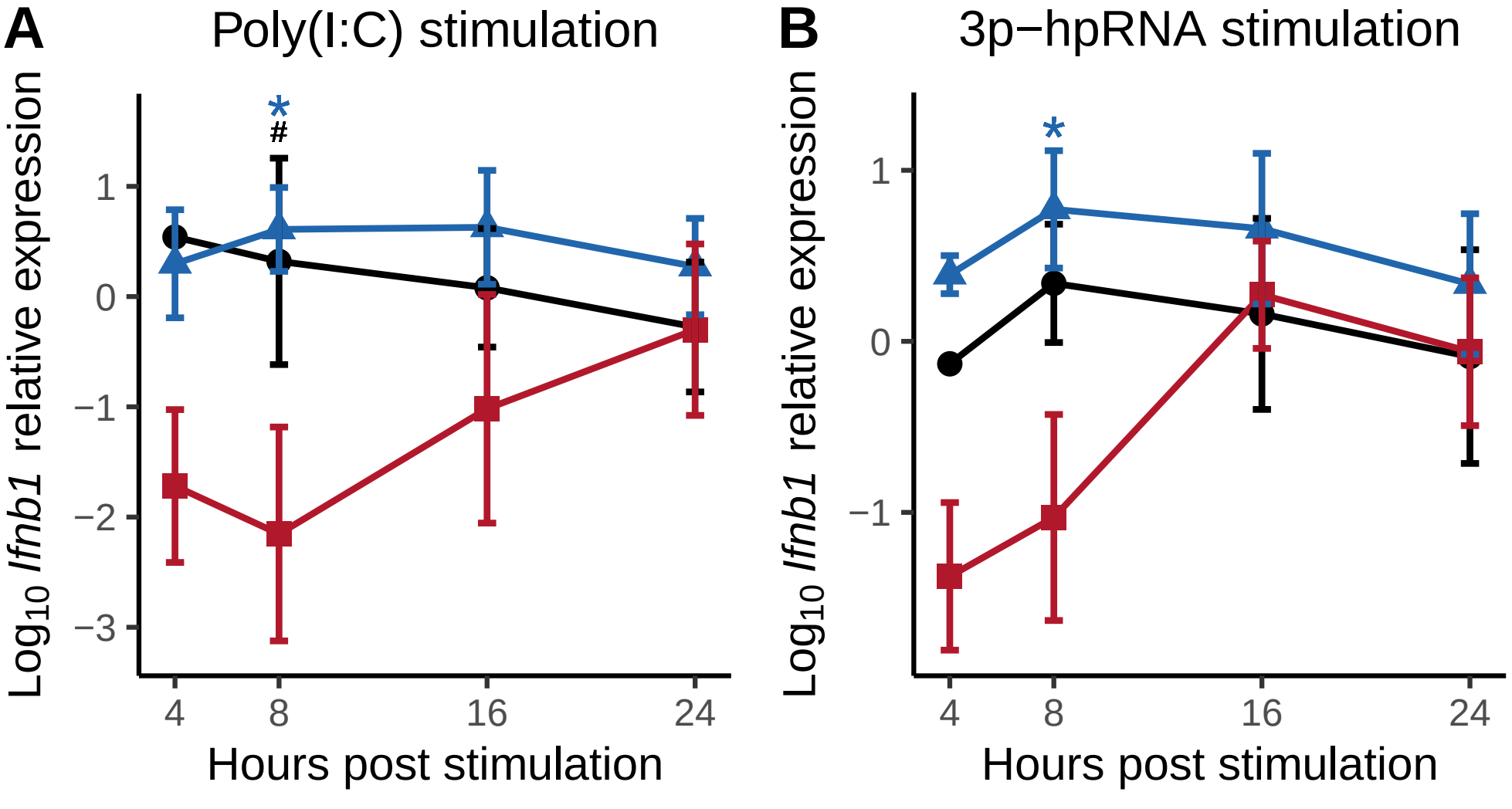
A
Poly(I:C) stimulation
B
3p−hpRNA stimulation
Log10 Ifnb1 relative expression
1
0
−1
−2
−3
*
#
4
8
16
24
Hours post stimulation
Strain
B6
CC001
CC071

Figure S2

A

Number of upregulated genes

| Time | B6 | CC001 | CC071 |
|---|---|---|---|
| 16h | 48 | 160 | 1 |
| 24h | 195 | 821 | 9 |
| 32h | 384 | 971 | 38 |

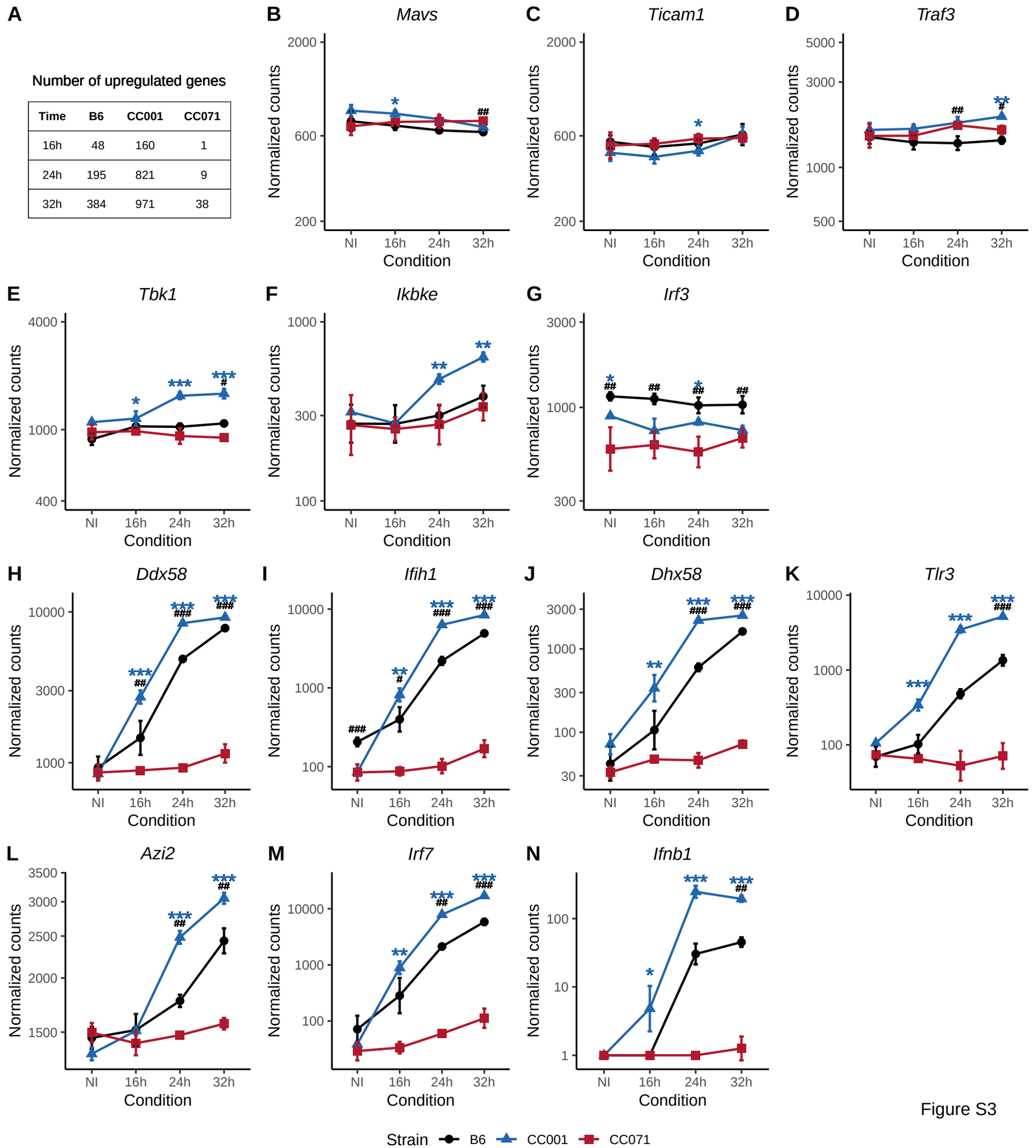


Figure S3

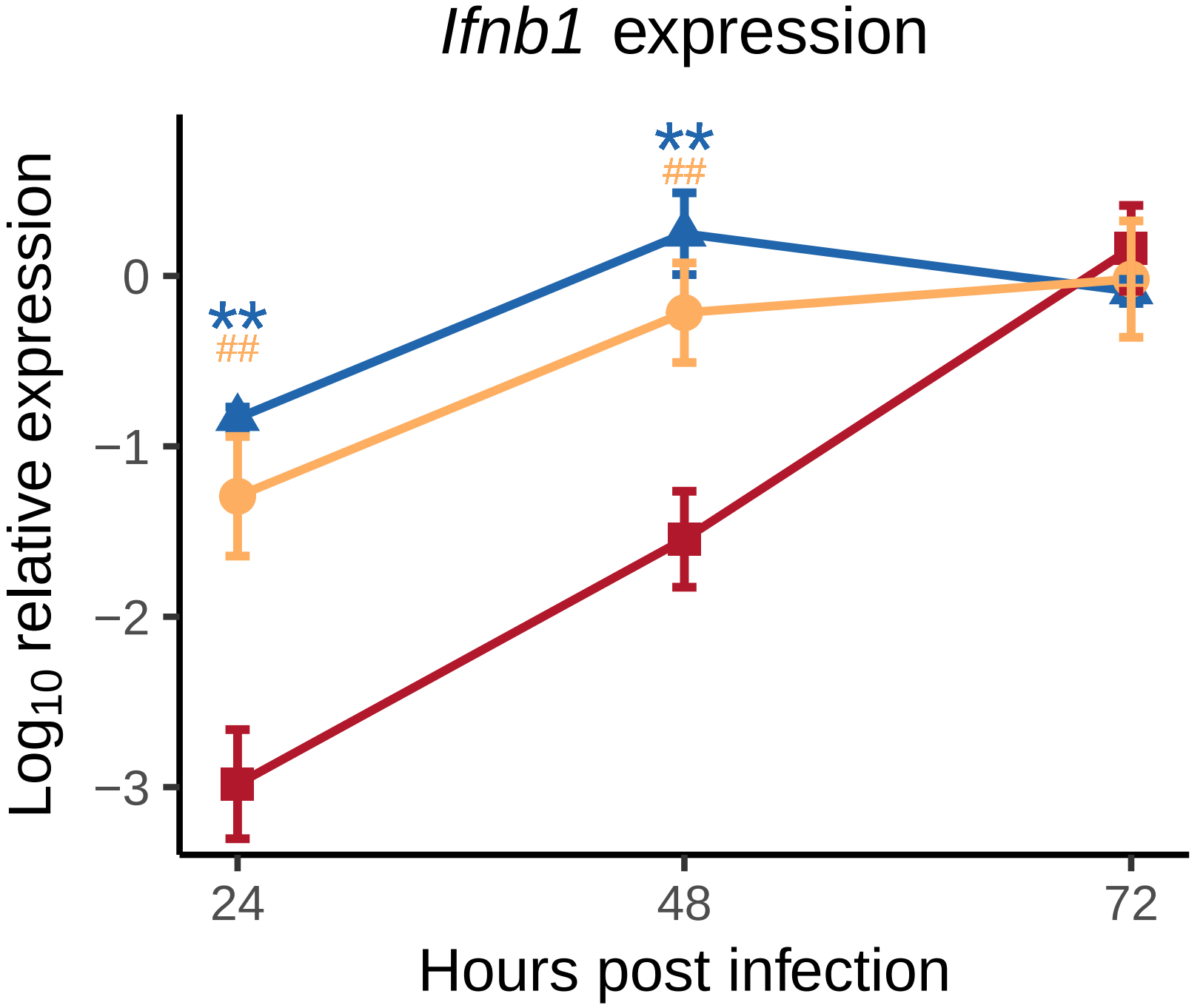


Strain

CC001 (n=3)

CC071 (n=3)

(CC001xCC071)F1 (n=3)

Figure S4

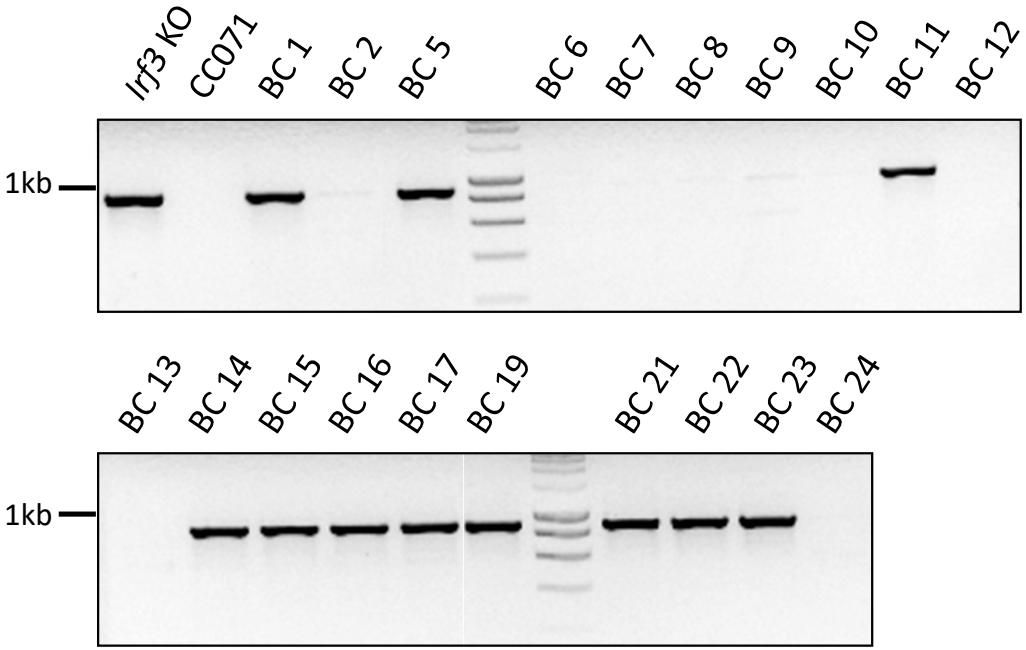
Irf3 KO
CC071
BC 1
BC 2
BC 5
BC 6
BC 7
BC 8
BC 9
BC 10
BC 11
BC 12
1kb
BC 13
BC 14
BC 15
BC 16
BC 17
BC 19
BC 21
BC 22
BC 23
BC 24
1kb

Figure S5

| **Gene** | **Forward** | **Reverse** |
|---|---|---|
| qPCR | | |
| *Ifnb1* | CAGCTCCAAGAAAGGACGAAC | GGCAGTGTAACTCTTCTGCAT |
| *Ifnα4* | TGATGAGCTACTACTGGTCAGC | GATCTCTTAGCACAAGGATGGC |
| ZIKA *Env* | CCGCTGCCCAACACAAG | CCACTAACGTTCTTTTGCAGACAT |
| *Ifitm3* | ACTGTGATCAACATGCCCAGAG | CTTCCGATCCCTAGACTTCACG |
| *Tbp* | AGAACAATCCAGACTAGCAGC | GGGAACTTCACATCACAGCTC |
| PCR genotyping | | |
| *Irf3* | CACTCCCACGCCTTCTGG | ACAAGCCTCTTGACCCATGG |

S1 table

**Immunofluorescence antibodies**

| Primary/secondary | Antibody | Species | Dilution | Reference |
|---|---|---|---|---|
| Primary | ZIKV envelop protein | Mouse | 1:200 | 4G2 antibody from ATCC hybridoma |
| Primary | Phosphorylated IRF3 | Rabbit | 1:250 | Cell Signaling Technology Cat#29047 |
| Secondary | Anti-rabbit AlexaFluor-488-conjugated IgG | Goat | 1:500 | Invitrogen Cat#A-11034 |
| Secondary | Anti-mouse AlexaFluor-594-conjugated IgG | Donkey | 1:500 | Invitrogen Cat#A-21203 |

**Western blot antibodies**

| Primary/secondary | Antibody | Species | Dilution | Reference |
|---|---|---|---|---|
| Primary | IRF3 Cter | Rabbit | 1:1000 | Cell Signaling Cat#4302 |
| Primary | Vinculin | Rabbit | 1:1000 | Proteintech Cat# 26520-1-AP |
| Secondary | Rabbit IgG HRP Linked Whole Ab | Donkey | 1:10,000 | Sigma Cat# GENA934-100UL |

S2 table